**CAPITAL UNIVERSITY OF SCIENCE AND
TECHNOLOGY, ISLAMABAD**

Image Fusion in Spatial Domain using Local Binary Pattern

by

Shahbaz Khan

A thesis submitted in partial fulfillment for the
degree of Master of Science

in the
Faculty of Computing
Department of Computer Science

2020

This work is devoted to my beloved Teachers, Family and Friends. I have a special feeling of gratitude for my beloved parents, sisters and wife. I would like to thank my supervisor for his firm belief and confidence that enabled me to reach this milestone.

CERTIFICATE OF APPROVAL

Image Fusion in Spatial Domain using Local Binary Pattern

by

Shahbaz Khan

(MCS171009)

THESIS EXAMINING COMMITTEE

S. No.	Examiner	Name	Organization
(a)	External Examiner	Dr. Ayyaz Hussain	QAU Islamabad
(b)	Internal Examiner	Dr. Shahid Iqbal Malik	CUST Islamabad
(c)	Supervisor	Dr. Abdul Basit Siddiqui	CUST Islamabad

Dr.Abdul Basit Siddiqui
Thesis Supervisor
November, 2020

Dr. Nayyer Masood	Dr. Muhammad Abdul Qadir
Head	Dean
Dept. of Computer Science	Faculty of Computing
November, 2020	November, 2020

Author's Declaration

I, **Shahbaz Khan** hereby state that my MS thesis titled "**Image Fusion in Spatial Domain using Local Binary Pattern**" is my own work and has not been submitted previously by me for taking any degree from Capital University of Science and Technology, Islamabad or anywhere else in the country/abroad.

At any time if my statement is found to be incorrect even after my graduation, the University has the right to withdraw my MS Degree.

(Shahbaz Khan)

Registration No: MCS171009

Plagiarism Undertaking

I solemnly declare that research work presented in this thesis titled "**Image Fusion in Spatial Domain using Local Binary Pattern**" is solely my research work with no significant contribution from any other person. Small contribution/help wherever taken has been dully acknowledged and that complete thesis has been written by me.

I understand the zero tolerance policy of the HEC and Capital University of Science and Technology towards plagiarism. Therefore, I as an author of the above titled thesis declare that no portion of my thesis has been plagiarized and any material used as reference is properly referred/cited.

I undertake that if I am found guilty of any formal plagiarism in the above titled thesis even after award of MS Degree, the University reserves the right to withdraw/revoke my MS degree and that HEC and the University have the right to publish my name on the HEC/University website on which names of students are placed who submitted plagiarized work.

(Shahbaz Khan)

Registration No: MCS171009

Acknowledgements

I am thankful to **ALLAH Almighty** who gave me strength to complete this work. After that, i am thankful to my parents and my family for their continuous support to achieve this goal. i would like to express my deep sense of respect and gratitude towards my supervisor **Dr. Abdul Basit Siddiqui** who has been guiding force behind this work. I am greatly obligated to him for his constant encouragement, invaluable advice and for propelling me further in every aspect of my academic life. His presence and optimism have provided an invaluable influence on my career and outlook for the future. I consider it my good fortune to have an opportunity to work with such a wonderful person.They are my role model of my life.

I also extend my thanks to all faculty members and staff of the Department of Computer Science, Capital University of Science and Technology, Islamabad who have encouraged me throughout the course of Master Degree. I am especially indebted to my parents for their love, sacrifice and support. They are my first teacher and role model of my life.

(Shahbaz Khan)

Registration No: MCS171009

Abstract

The focal length of optical devices is limited. A camera focuses only on those objects which lie in its focus range, where all other objects are appeared as non-focused or blurry. Image fusion is a process which combines two or more input images to create a fused image which contain maximum focus area. For a task of image restoration, where one has to segment an input image into focused and non-focused regions by using a specific segmentation algorithm. In this research LBP based blur measure operator is used to segment an input image into blurred and sharped regions using multiple thresholds over multiscale environment. To evaluate this metric, a detailed dataset of multi-focus images is required. For this purpose, a dataset containing twenty five multi-focus images is collected to create complimentary fused images. A fused image is evaluated using four quality metrics such as Gradient, Normalize Mutual Information, Yang and Chen blum metrics. As per experimental evaluation, this technique has outperformed previously proposed state of the art techniques.

Contents

List of Figures

List of Tables

Abbreviations

CNN   Convolution Neural Network

DNN   Deep Neural Network

DSIFT   Dense Scale Invariant Feature Transform

GF   Guided Filter

LBP   Local Binary Pattern

MSIFS   Multi Sensor Image Fusion System

NSCT   Non-subsampled Contourlet Transform

SR   Sparse Representation

SSIFS   Single Sensor Image Fusion System

Symbols

$Img_b(i,j)$	Pixel values of Image
(i,j)	Single pixel value of image
$S_A^x(i,j)$	Vertical Sobel Operator
$\alpha - matte$,$\alpha_((i,j)$	Significance of pixel location (i,j)
$Mask^i(i,j)$	Alpha maps of vector initialization
L	Laplacian matrix of matting
h^3	Sharpness map at the largest scale
$Z^{AF}(i,j)$	Gradient of the input image A

Chapter 1

Introduction

1.1 Overview

Image processing is a new technology which can be applied in a real-world in future decades. In image processing, different images can be employed to extract desired results. Image processing techniques are classified into analog and digital image processing techniques. Analog image processing deals with photographs and printouts, meanwhile digital image processing deals with digital images. Digital images are composed of multiple pixels oriented grid-like structures containing n rows and m columns. Each image pixel contain an intensity value, captured at that particular point. Lets consider Y as an input image and (i,j) are the coordinates of any pixel. The image is signified as a function of location: $Y(i, j)$, where i and j are positive integers. Thus an input image $Y(i, j)$ is a generalized matrix of pixels. In image processing, different type of operations can be applied on input images to create an output image with desirous information [1]. To perform a particular operation on an input image, the image must be segmented into focused and out of focused regions. There are multiple types of features which can be significantly employed to classify blurred and sharpened regions. A sharpened image contains more spatial detail as compared with blurry input image. However, in most of the cases, it is not possible to obtain an all in focused output image. Different type of

problems can occur during capturing an image. One of the main problems is that a short focal length of a capturing device, results ambiguous situations where limited number of regions are in focused and rest of the parts are out of focused. To create an all in focused output image, multi-focus image fusion can be performed using a certain number of operations. In image processing, it is generally required to have a well-focused input image while performing a relevant task such as image enhancement, segmentation, watermarking etc.

In a fusion process, multiple input images are combined into a single enhanced output image. Similarly, Multi-focus image fusion can be used to collect valuable facts from multi-focus input images[1].Image fusion is a process of combining focused regions of input images and reconstruct an all in focused new image with higher focused regions. Image fusion is a considered as a better approach, where spatial information can be increased by extracting spatial details from the input images. Image fusion is an effective and suitable method for machine/human observation based multiple applications, such as remote sensing (panchromatic, multi-spectral), medical images, target recognition, object detection and image segmentation [2].

Image fusion can be employed for Target recognition, where multiple sensors are used to capture scene images. When data is redundant, the parts of an input image are not in focus, which significantly drops precision of a recognition system . In the case of image segmentation, different regions of an image are segmented to find out a region of interest. if segmented regions are blurry due to any reason, then efficient segmentation is not possible. Multiple images sensors contain different type of geometric demonstrations, which are to be converted to have a common depiction for fusion.

Images can be fused in the frequency domain and also in the spatial domain. In the spatial domain, input images divided into block type regions and merged sharper blocks and provide better image fusion performance [3][4].

The focused regions contain all in focused captured detail whereas de-focused regions contain a low focused detail because of blurriness. Figure 1.1 shows a foreground and background pair of multi-focus images.
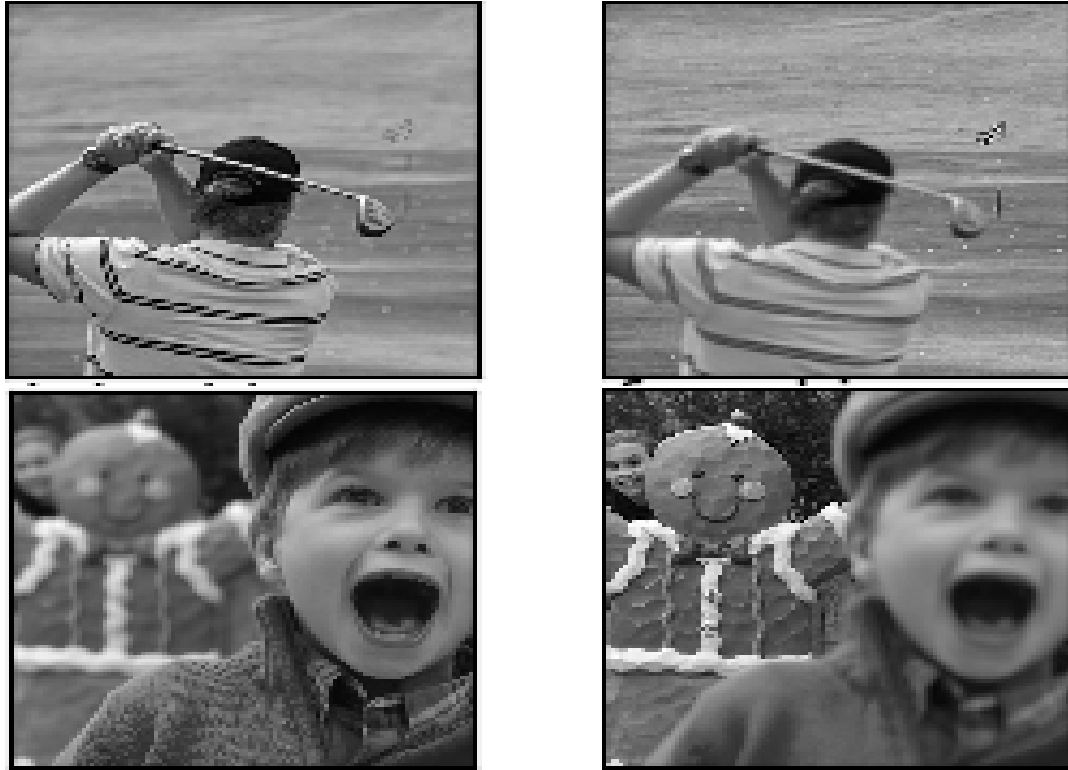
FIGURE 1.1: Foreground and Background Focused Images.

When an image of a scene is captured, usually the objects at the greater focal length of the camera get blurred and if the objects at greater length are focused, the objects at short focal length get blurred. In another case, if the objects in the scene are moving, they get also partially blur. In such a situation, it is required to generate an image that shows all the objects are in focus. It is very hard to take an image that contains all the focused objects. In many cases, the reference or source image is not present. A reference image is a completely focused image. if source images are not present, then the task of creating an all-in focus image becomes more complex and it is called blind image fusion.

Many techniques split the source images into the blocks which later select the sharper blocks from an input image and compute the fused image. Many image fusion techniques are present like PCA, DCT, DWT [4]. The transformation of the image by using the computational equation is called the frequency-domain method. The frequency-domain method is depending on changing the Fourier

transform of an image.

Roughly, the term frequency in an image tells about the rate of change of pixel values. Many techniques are available to perform image fusion like high pass filtering(HPS) technique. There are some other methods which are Discrete Wavelet Transform(DWT), Laplacian pyramid(LP) and uniform rational filter bank(URFB).

1.2 Single Sensor Image Fusion System

Single sensor image fusion system has presented the process which captured the real-world images in order. They compute a new image with maximum information content by combining all the sequences of the image. It has some drawbacks due to the competency of sensors like variant and noisy environment. This process is shown in figure 1.2 [3].
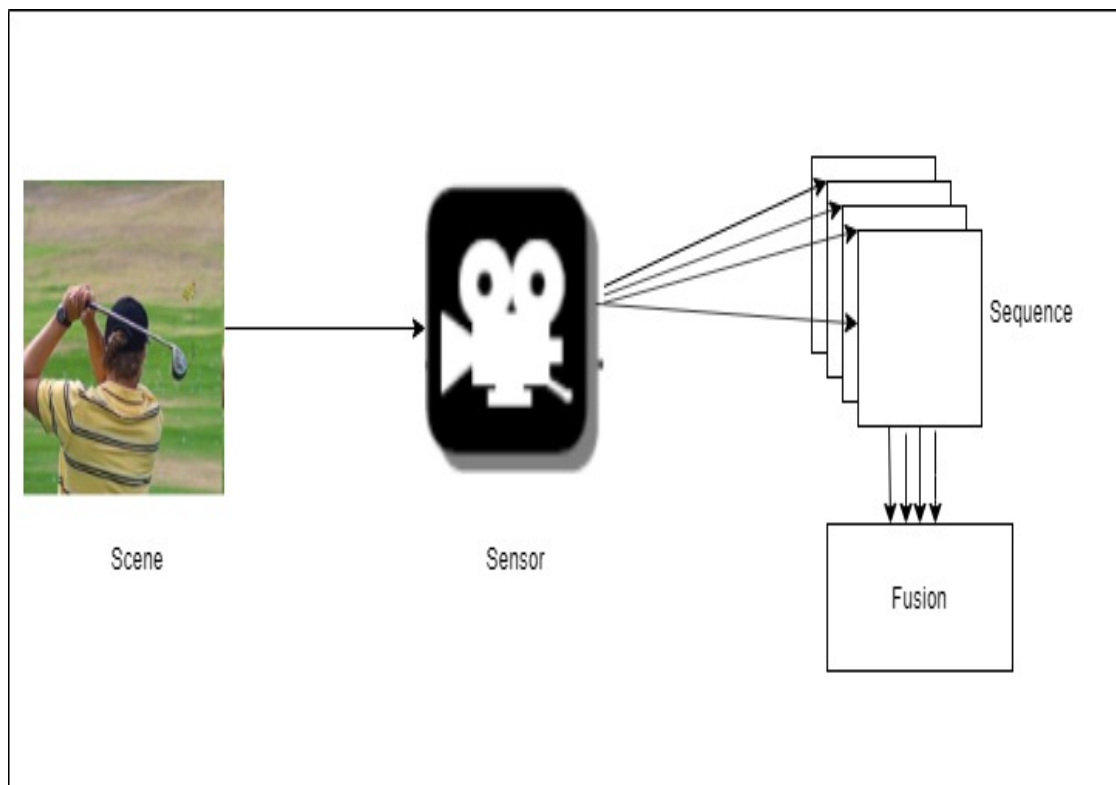
FIGURE 1.2: Single Photographic Sensor based Image Fusion .

1.3   Multi Sensor Image Fusion System

Single sensor image fusion limitation overcome by multi sensor image fusion. In multi sensor image fusion, the fused image is produced by passing the input image from many sensors. The images of two different cameras (like an infrared camera and digital camera) are syndicate to form a fused image. The digital camera is best for the daylight scene and the infrared camera provides the best result in case of a poorly illuminated environment. Multi-sensor image fusion provides the best result and overcomes the limitation of single sensor image fusion in Figure 1.3 [3].
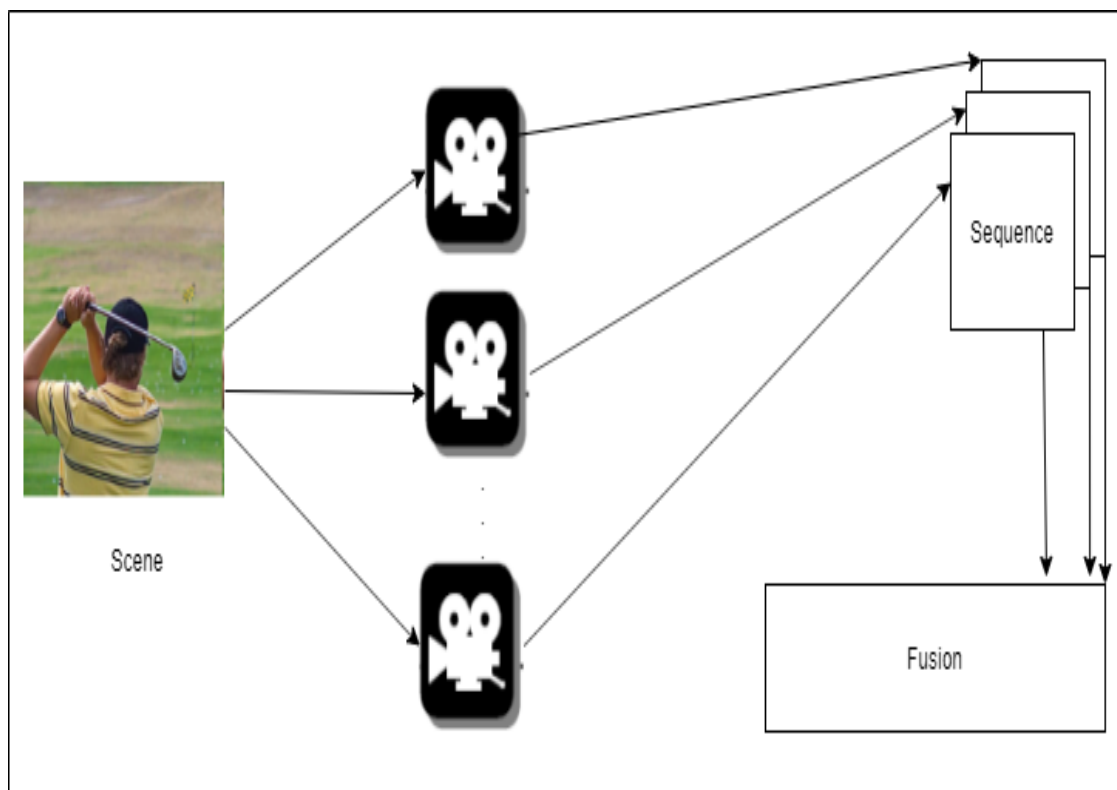
FIGURE 1.3: Multi Photographic Sensor based Image Fusion.

1.4   Levels of Image Fusion

Image fusion can be performed at three levels which are Pixel level, feature level, and decision level. All three levels of image fusion are [5] discussed in figure 1.4.
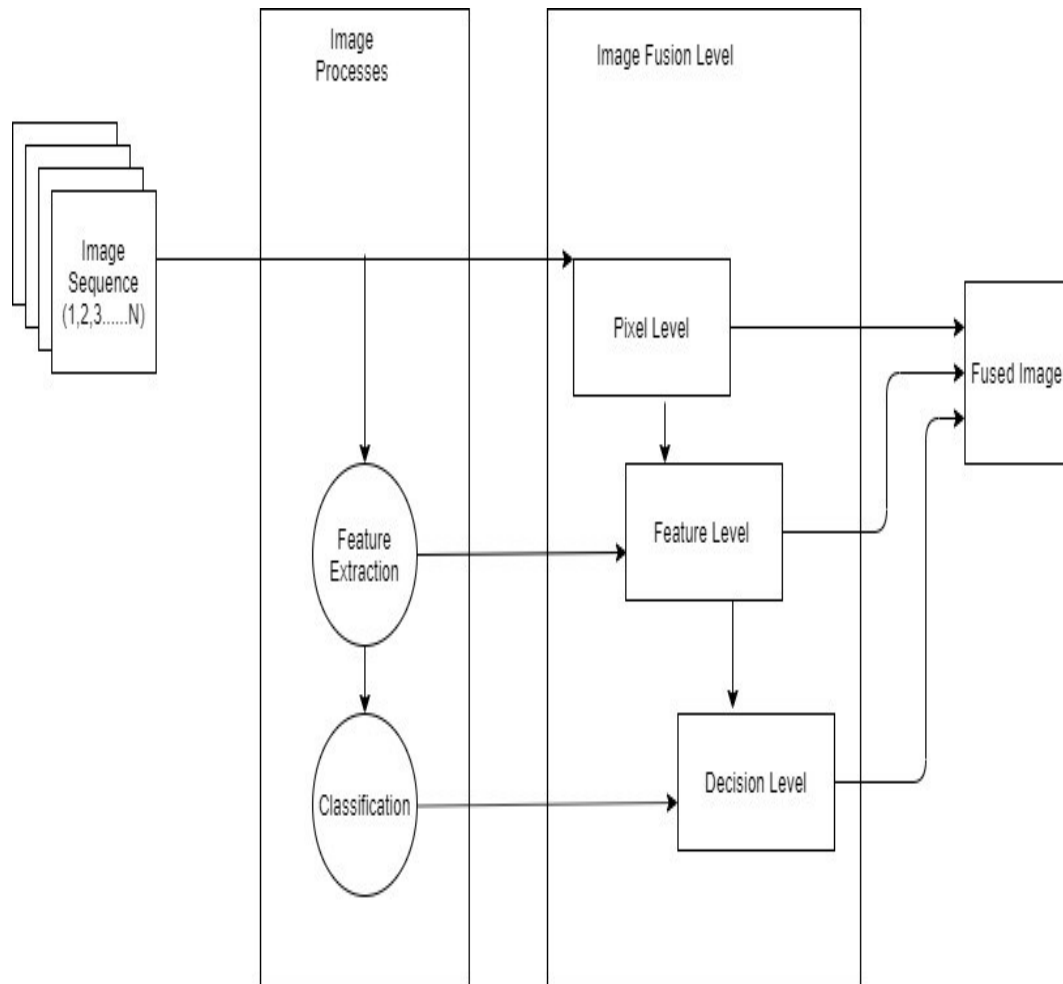
FIGURE 1.4: Image Fusion at Pixel Level.

1.4.1 Pixel Based Low Level Image Fusion

Pixel-based low level directly operates on the pixel of the image [1]. In the case of a low-level source image signals are joined to form a new fused image signal. The Pixel-based level depends on the spatial domain method of multi-focus image fusion [4][5][6].

1.4.2 Feature Based Middle Level Image Fusion

The Feature-based middle level operates different features of the image such as edge, region, shape, length, and direction. The Feature-based middle level is also

known as the object level. Object-level computes the feature and object extracted from the input image [4][5][6].

1.4.3   Decision Based High Level Image Fusion

A decision-based high level is taken as a symbol level which operates at an actual point. Object-level performs probabilistic decision information of the fusion process which can be achieved by decision-maker operations on the results of feature level [4][5][6].

1.5   Techniques of Image Fusion

There are multiple techniques which can be employed for image fusion such as spatial and frequency domain image fusion.
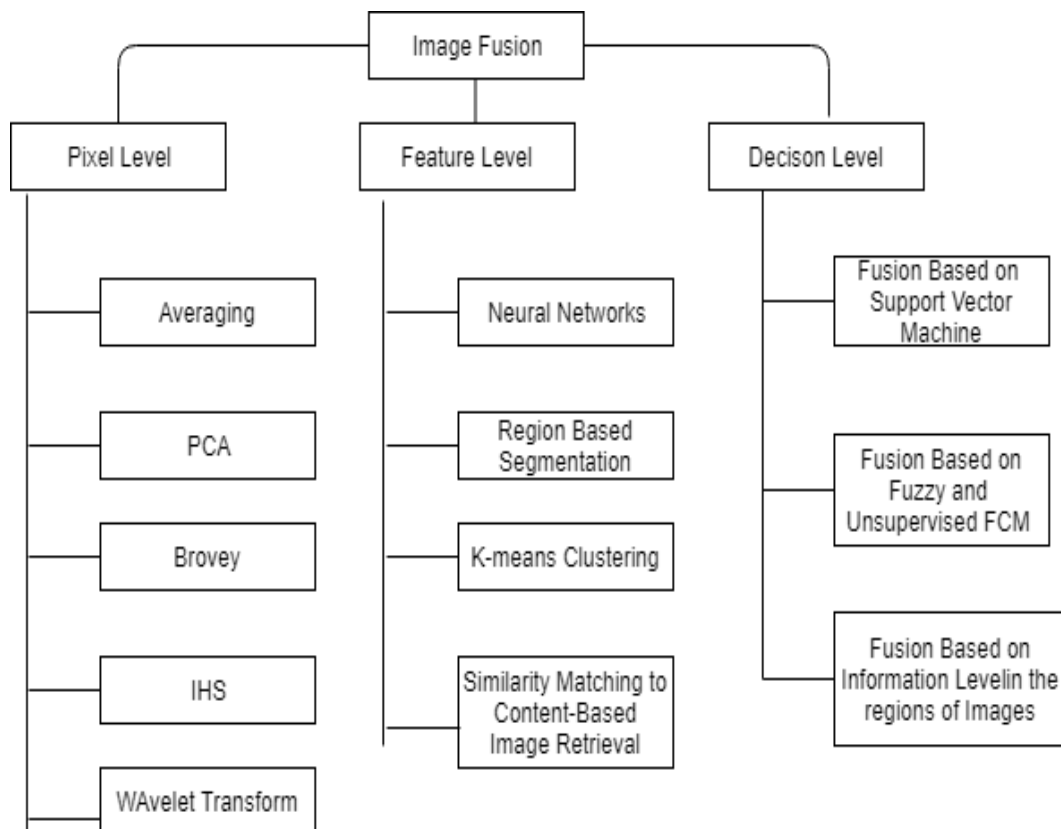
FIGURE 1.5: Multiple Techniques of Image Fusion at Various Levels.

1.5.1 Spatial Domain Image Fusion

Spatial domain methods are refered as simple image fusion methods. In the case of the spatial domain, input images are divided into focus and out-of-focus blocks. All the focus blocks are combined to produce a better-fused image. The transformation of the number of correlated variables and uncorrelated variable by using Principal Component Analysis (PCA) which is used for image classification and image solidity [3][4]. The Spatial domain method contains many techniques for image fusion like (simple average, maximum, minimum, Min-Max, etc). A simple average is very reliable to compute the fused image. The final image is computed by selecting the max or min pixel form the input images.

In the spatial domain, every pixel of the image is based on its neighbor pixel. Let us consider one-pixel $Pixel(i, j)$, its nearing pixels are added and calculated the block average. Due to some limitations, these methods are not best for real-time applications. Some other techniques are present in spatial domain techniques. In the weighted averaging method, many weights are applying to all input images. This technique improves the reliability and detection which increased the SNR of the fused image. PCA changes the remarks of probably correlated variables into a set of values of the uncorrelated variable. Intensity Hue Saturation (IHS) is a color space simple and high sharpening ability. Intensity is formed by different RGB bands.

1.5.1.1 Simple Maximum Method

In the case of a simple maximum method, the maximum intensity of a pixel is selected from input images for reconstruction of a fused image [1][4].

$$F(i,j) = \sum_{i=1}^{N} \sum_{j=1}^{M} max(X(i,j), Y(i,j)) \tag{1.1}$$

X and Y are original images and F is a Final image.

1.5.1.2 Simple Minimum Method

: In the case of a simple maximum method, minimum intensity of a pixel is selected from source images for reconstruction of a fused image [1][4].

$$F(i,j) = \sum_{i=1}^{N} \sum_{j=1}^{M} min(X(i,j), Y(i,j)) \tag{1.2}$$

where X and Y are original images and F is a Final image.

1.5.1.3 Principle Component Analysis

PCA is a statistical type feature that is used for mean centering and normalizes the data of each attribute by using Eigen Value decomposition [7]. PCA algorithm used the following steps for calculation. First of all, create a column vector of the source images and then compute the covariance matrix of both column vectors. The diagonal elements hold the change of each column vector. Then compute the Eigenvectors and also compute the Eigenvalues of the covariance matrix. Every element is divided with the mean of the Eigenvector and larger Eigenvalue normalized the column vector. Every pixel of the images multiplies with the value of normalizing Eigenvector which performs as the weight values. 7) fused image matrix is computed with the addition of two scaled matrices [1][4].

1.5.1.4 Guided Filter

The source image and fused image have a direct relationship in a local square kernel with center pixel.

$$F_{ij} = a_{tu} * S_{ij}, (i,j) \in W_{tu} \tag{1.3}$$

As we know S_{ij} Shows the pixel value at the location (i, j) of the source image S. F_{ij} is the resultant fused image of S_{ij}. (i, j) and W_{tu} indicates the position of

the pixel. S_{ij} is inside the square kernel W_{tu}. a_{tu} and b_{tu} are the constant values in the square kernel W_{tu}. after that, they calculated through reducing the square difference between F and the source image S. The corresponding formula is given by the following [8].

$$E(a_{tu}, b_{tu}) = \sum_{i,j=W_{tu}} ((a_{tu} * S_{ij} + b_{tu} - P_{ij})^2 + \epsilon * a_{tu}^2) \qquad (1.4)$$

1.5.2 Types of Spatial Domain Image Fusion

There are many types of spatial domain image fusion.Some important are shown in figure .
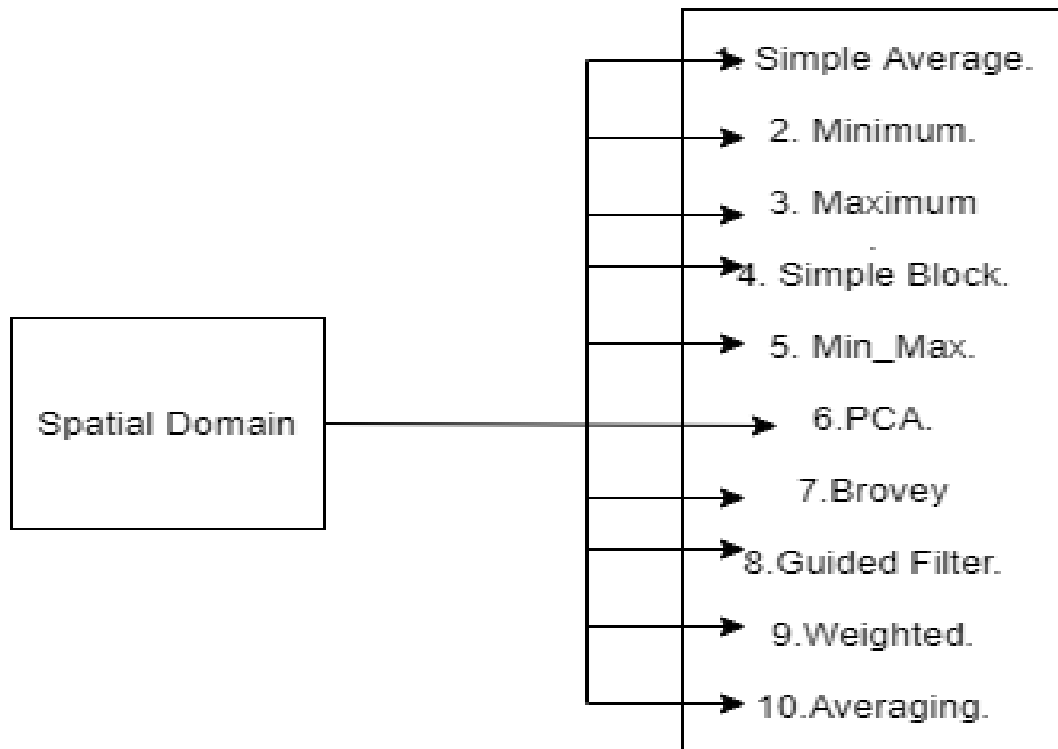
FIGURE 1.6: Types of Spatial Domain Image Fusion.

1.5.3 Frequency Domain Image Fusion

Input images are decomposed into a multi-scale coefficient in the frequency domain [9]. There are many techniques, for the selection and manipulation of these

coefficients. Image registration is an important step for the fusion process. The transforming of multiple sets of data into a single system is known as image registration [10]. In the frequency domain, the input image is convolved into a Fourier domain and this process is done by using a frequency filter. After that Frequency filter returns to the original domain by applying inverse transformation without losing any information [4][6].
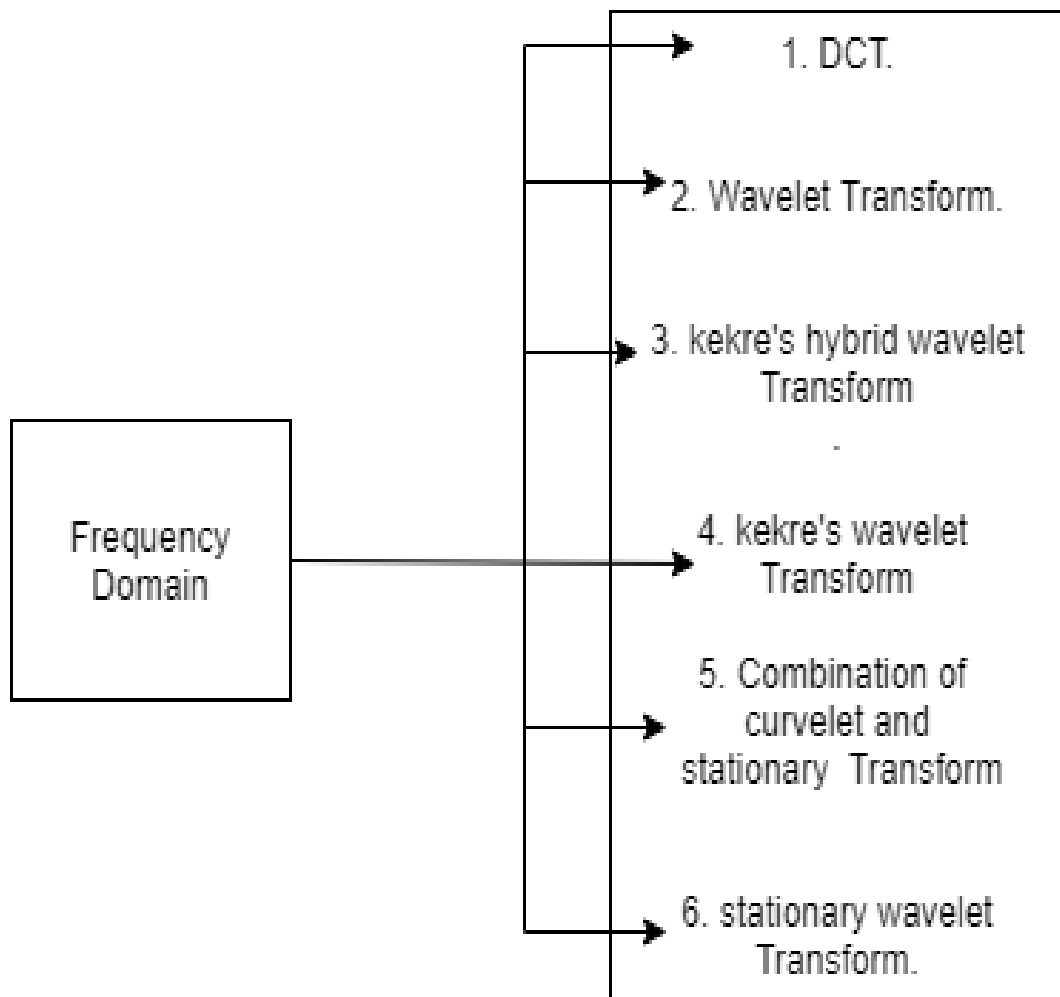
FIGURE 1.7: Types of Image Fusion in Frequency Domain.

1.5.3.1 Discrete Cosine Transform

Discrete cosine transform is used for multi focus image fusion which are belong to frequency domain of image fusion.

DCT is a discrete cosine transform.

1. Import the input images.

2. Apply DCT in the source image in blocks of 8x8.

3. Calculate the DCT component average.

4. Calculate the inverse DCT.

5. Calculate the fused image by using the below equation

$$z(m,n) = \sum_{m=1}^{N}\sum_{n=1}^{N} \frac{2\alpha(m)\alpha(n)}{N} d(m,n) \cos[\frac{(2i+1)\pi(m)}{2N} \cos[\frac{(2i+1)\pi(m)}{2N}] \quad (1.5)$$

1.6 Problem Statement

In multi-focus image fusion the task of creating an all in focus image becomes challenging in order to use the images in various applications such as remote sensing, medical images, target recognition, object detection and image segmentation etc. The results of fusion primarily are based on segmentation of input images into their focused and non-focused regions. Different techniques have been reported in the literature to obtain a fully focused image. For better fusion results of multifocus images the existing approaches can be further improved by using texture based features such as local binary patterns (LBP).

1.7 Research Questions

This study has been conducted around the following research questions.

Q1: What is the effect of blurriness on the texture of different local regions of an image ?

Q2: How blurriness effect local binary patterns in an image?

Q3: How LBP on local binary patterns can be used to create a fused image?

Q4: How LBP can be used to segment focused and non-focused regions?

Q5: How fused image can be generated from the segmented images?

1.8 Thesis Organization

This thesis is organized in following five chapters which are introduction, literature review, methodology, experimental setup results and discussion, and Conclusion.The introduction chapter describes the image fusion techniques, image fusion types and image segmentation methods. The literature review chapter describes the different methods of image fusion which are discussed in previous papers like: (1) convolution neural network, (2) sparse representation, (3) discrete wavelet transform and (4) dense scale-invariant feature transform etc. The methodology chapter describes our techniques of image fusion. In methodology section image fusion in spatial domain using local binary pattern are briefly described. The experimental setup results and discussion chapter describes the result of our experimentation which contain comparing table, comparing graph and images results with different other techniques which contain sparse representation, deep neural network and guided filter etc. Finally, conclude the results in conclusion section.

Chapter 1	Introduction
Chapter 2	Literature Review
Chapter 3	Methodology
Chapter 4	Experimental Setup Results and Discussion
Chapter 5	Conclusion

Chapter 2

Literature Survey

2.1 Literature Review

Many techniques have been proposed by researchers in the area of multi-focus image fusion. A list of techniques presented in recent literature is given as follows.

Morris et. al [4] proposed the combination of images from different sources to produce a better visualization and a more informative image than the input image. Different RGB values are computed from many fusion techniques. The proposed technique is the combination of simple spatial and principle component analysis base fusion techniques called novel optimized mixed spatial fusion approach. The proposed technique extracts better results than the single spatial approach. They optimized the Novel optimized mixed spatial fusion technique by using partical swarm optimization. The swarm of particles move in the search space and produce a better solution.

Morris et al [4] proposed a mixed split image approach in which each image is divided into four sub-images and then applied the fusion method. They used a fixed-size block. In the end, simple maximum, simple minimum and principle component analysis sub-images are applied in particle swarm optimization. Finally, they computed different parameters using signal to noise ratio, peak signal to noise ratio, mean square error and mean deviation.
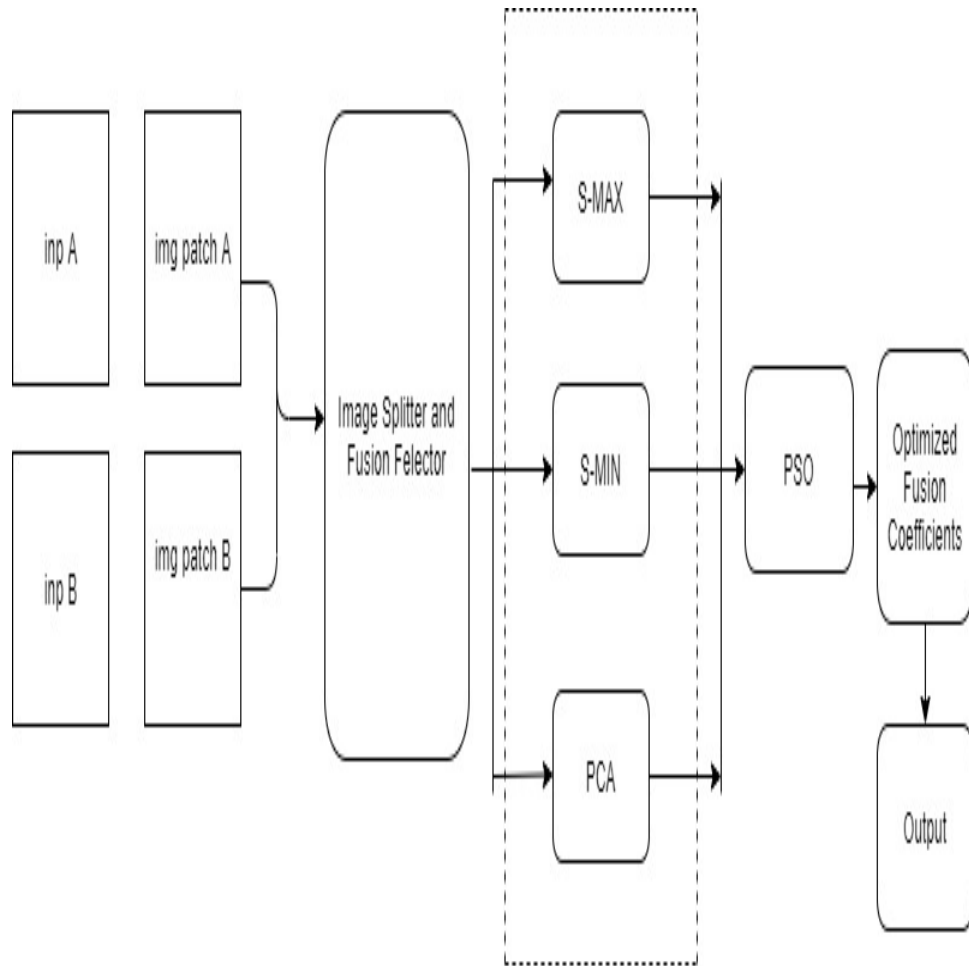
FIGURE 2.1: Mixed Split Based Image Fusion Approach.

The resultant image is and more informative than the input images. Multiple images are combined to get a fused image. Abhyankar et al [11] performed the fusion process and computed the resultant image. The fusion process uses two levels, pixel-based and decision-based. Novel image fusion methods use the first-order derivative while composing the constituent image into sub-images. The proposed technique reduces the mathematical complexity for image fusion and finds the edge along x and y direction using a Sobel operator. The Sobel operator provides resistance against the noise and is compared with the Prewitt operator. They calculated the edge of the image and provided as an input to the genetic algorithm for computing the weights. The combination of Gaussian smoothing and differentiation are known as Sobel operator. It provides both directions and magnitude of the edge at a specific point. After calculating the mean and standard deviation of

the edge, they formed the feature vector of the edge. After that, they applied the genetic algorithm. Selection is made by using the highest fitness value. After the selection process, uniform crossover and bit-flip mutation are applied to replace the existing population. Afterward, they extracted the final fused image. These results are mostly similar to the results of Discrete Wavelet Transform (DWT) for RMSE, PSNR, and SSIM. The entropy, image quality index, and mutual information values are improved through their technique.

Anbarjafari et. al [12] presented a new super-resolution method. The number of pixels increased in digital images is known as interpolation. This technique is based on the interpolation of the frequency sub-bands image. They [12] increased the quality of the task. They used the bicubic interpolation technique. They decomposed the image into different sub-bands by using DWT. Edges are detected through an edge detection algorithm. The combination of input low-resolution image and high-frequency sub-band images extract a new super-resolved image by using inverse DWT. The proposed (Demirel-Anbarjafari Super Resolution) DSAR technique which can be computed by DWT. They used many image datasets for testing the proposed techniques. PSNR showed the superiority of this proposed technique over other image improvement techniques. The value PSNR using the Lena image dataset is 7.93, which is greater than the cubic interpolation.

The objects of the single image cannot be viewed sharply because of the limited depth of field. Aslantas et al [13] combined multiple images of the same sight to produce a sharp image that contains maximum information. Aslantas et al [13] utilized the Artificial Bee Colony optimization algorithm (ABC) to improve the performance of the spatial domain image fusion technique. In the case of the spatial domain, multi-focus images are distributed into block type regions. Sharper blocks are merged into a single fused image [14]. They used the Sobel operator to evaluate the edge and calculate the orientation and magnitude of the pixel. The population depends on the total number of working bees, equal to the number of solutions. The population is distributed uniformly and the cycle is repeated in the search processes of the employed, onlooker, and scout bees. The defocus parts of the image are decomposed into the block and then it is replaced with the sharper

part of other same images to construct a fused image. They take two image sets, Board and Lab. They calculated the image fusion quality metrics, which are Variance (VAR) and Objective Edge Based Measure (QE). Results of the Artificial Bee Colony (ABC) Algorithm are more powerful than the DWT and Laplacian Pyramid.

Chang et al [15] showed an effective algorithm for image fusion using Laplacian pyramid method. They used the resolution signal decomposition scheme, based on fusion strategy to decompose the source image into sub-images. They used a fixed block size. Chang et al [15] presented three steps. First of all, each source image of the Laplacian pyramid is deconstructed separately and then different fusion rules are applied. Maximum region information rule can be extracted from top-level while at rest level they extracted maximum region energy rule. Finally, they obtained fused image using inverse Laplacian pyramid transform. They performed tests on set of images. The set of images are Clock Images and Metallurgical Images. They evaluated the proposed technique by comparing with some other techniques. They performed comparison with some common methods namely, Max method and Wavelet transform method. Their results showed that their proposed technique provides more accurate and better final images from the original images Zhang et al [16] proposed region-based multi-focus image fusion scheme. They used quality evaluation of Genetic algorithm and spatial domain. They performed feature and pixel-level fusion. When they considered the image, the source images is split into blocks and blocks are selected. The selected blocks are used to compute the quality of evaluation value in the final image. They must know the regions of the image is clear or not for computing the quality of the image [17]. They divided the image into blocks or lattice and captured the image quality of the local region. Zhang et al [16] applied GA and they calculated the fitness function and then performed crossover and mutation. GA is applied for the searching of optimal block size. They used a fixed block size. They used RMSE and similarity measure to improve the results. The results extracted from proposed method performed better than Haar Wavelet transform technique and morphological wavelet technique.

Jin et al [18] used a spatial frequency approach instead of the spatial domain. It is a process of fusing two images and compute a new image which has the best description known as Wireless visual sensor network (WVSN). They proposed an algorithm for multi-focus images or videos using DCT based standards in WVSN. They evaluated the performance of the proposed method under different evaluation metrics. They noted that the suggested method provided better image fusion. They implemented the simple and computationally effective method. In the case of wireless visual sensor networks, the source images are coded in JPEG format. Jin et al [18] proposed results are more accurate and more effective than previous Discrete Cosine Transform (DCT) based technique and state-of-the-art method.

Liao et al [19] proposed boundary aware multi-focus image by using a deep neural network to overcome the deficiency. They used out-of-focus and in-focus information of input images and contributed threefold. They applied two networks to handle many circumstances for ranges from long distance and near the focus and defocus boundary, respectively. Liao et al [19] overtook the state-of-the-art methods, both qualitatively and quantitatively. They applied some simple post-processing to produce the conclusion map from the refined score map. Finally, they applied the fusion on images by allowing the conclusion map to get the fused results.

Peng et al [20] used deep convolution neural network (CNN) for multi-focus image fusion. Manual design is a difficult task and also impossible to extract and perfectly design all the compulsory factors into account. They used activity level measurement and fusion instruction as two important features in multi-focus image fusion, to overcome these existing problems. They performed direct mapping between input images and the de-blur map. They performed four steps for this kind of image fusion: de-blur detection, primary segmentation, consistency authentication and fusion. In focus detection, if the image is a color image then it is converted into grayscale. On the other hand if the image is grayscale originally then it is kept grayscale. Peng et al [20] allotted the value of every coefficient to all pixels in the parallel patches and took average of the intersecting pixels for focus map. In case of initial segmentation, they adopted the choose-max method

to process, and 0.5 fixed threshold for segmenting the map into a binary map. The binary segmentation map is expected to hold some wrongly classified pixels which can be detached by using the small area for verifying the consistency. Finally, when the decision map is obtained, they computed the fused image with the weighted-average rule. In every image, an area all over the border between focused and out-of-focused parts is enlarged.

Liu, Y et al[21] proposed technique based on Multiscale transformation (MST) and sparse representation (SR). To overcome the flaws of both SR and MST fusion method, they combined both of them simultaneously. First of all, they used MST on the pre-registered original images and extracted the low pass and high pass coefficients. They merged the low passband with SR fusion approach, and the high passband is fused with absolute values of coefficients. This process is known as activity level measure. Liu, Y et al [21] obtained the final fused image by acting the inverse MST on the combined coefficients. They compared the fused results subjective and objective wise under the proposed framework and performed the best fusion results. The benefits of the proposed fusion framework is that it is used to observe theoretically and then can be verified through experiment. They performed experiments with six most famous multiscale transforms with different breakdown levels.

Liu et al [22] Multi-focus fused image is to produce the best activity level measures to calculate the clear original images. They performed the novel image fusion technique for multi-focus image dense-SIFT. The main purpose of novel image fusion technique is to demonstrate the great perspective of local features in which the dense SIFT is used for the fusion process. In the case of multiple input images, they increased the variety of the fused image. Local feature descriptor is used to match the un-registered pixels. Liu et al [22] used the sliding kernel technique. The amount of the activity level of source image patches is computed by dense SHIFT. These patches are used to compute the starting decision map. The decision map is developed by matching the feature and de-blur measure comparison. Final results show that the proposed technique can be reasonable and can find better results as compared to some the state-of-the-art fusion methods.

According to Huang et al [23], if every particle obtained is de-blur part of image then they have to take fused images under the same viewpoint, unlike different focal setting. Pyramid decomposition, multi-resolution transform and wave techniques are used to overcome this problem. Huang et al [23] proposed sparse representation in which source image shows the sparse coefficient, after that the coefficients are joined with the choose-max fusion rule[24]. The fused image is restructured from the additional combined coefficient and the vocabulary. Fusion method can resolve the image refurbishment and fusion problem by shifting the estimated standard in the sparse depiction algorithm. They evaluated the fused results with the SG, MWT, SWT, DWT and NSCT-based methods. They have studied only DCT based dictionary. However some other techniques are present like learning-based methods. The experimental results demonstrated that the proposed technique extracts valuable results in subjective and objective metrics.

Picture quality is a feature of an image to deal with the perceived image deprivation. Mishra et al.[25] performed comparison between perfect and faultless image. Image systems may establish some amount of distortion or artifacts in the signal. Their weakness is a quality estimation. Many quality metrics can be objectively measured and also evaluated by a program. Kang et al [26] distinguished a complete reference (FR) and Non-reference method (NR). In these methods of image quality measurement FR, the attribution of a trial image is measured by matching a mentioned image which is supposed to contain the ideal quality. Image with no reference is also computed through NR metrics

Wang et al [8] proposed the planned novel multi-focus image fusion to rely upon an arbitrary walk and guided filter. They used the optimization of the arbitrary walk and decay function for fusion. The arbitrary walk is promoted for weight map frankly. The eminence of an arbitrary walk and guided filter in image fusion are entirely appropriate by adaptable relative coefficients. The projected technique concludes six steps: first of all, they decomposed the images into detail level and base level with an arbitrary walk. Secondly, the weight maps are depending on arbitrary walk directly, and smoothing filters depend upon the guided filter. Thirdly, the weight maps and the foundation levels are obtained by collecting the

beginning weight maps in various size and ending weight maps are gained by using arbitrary walk for optimizing. Next, the fused detail level and foundation level are gained. In the end, the fused image is obtained by collecting the fused foundation level and the fused detail level. Wang et al [8] experimentally showed that the projected method accomplished subjective and objective improvement in many other techniques.
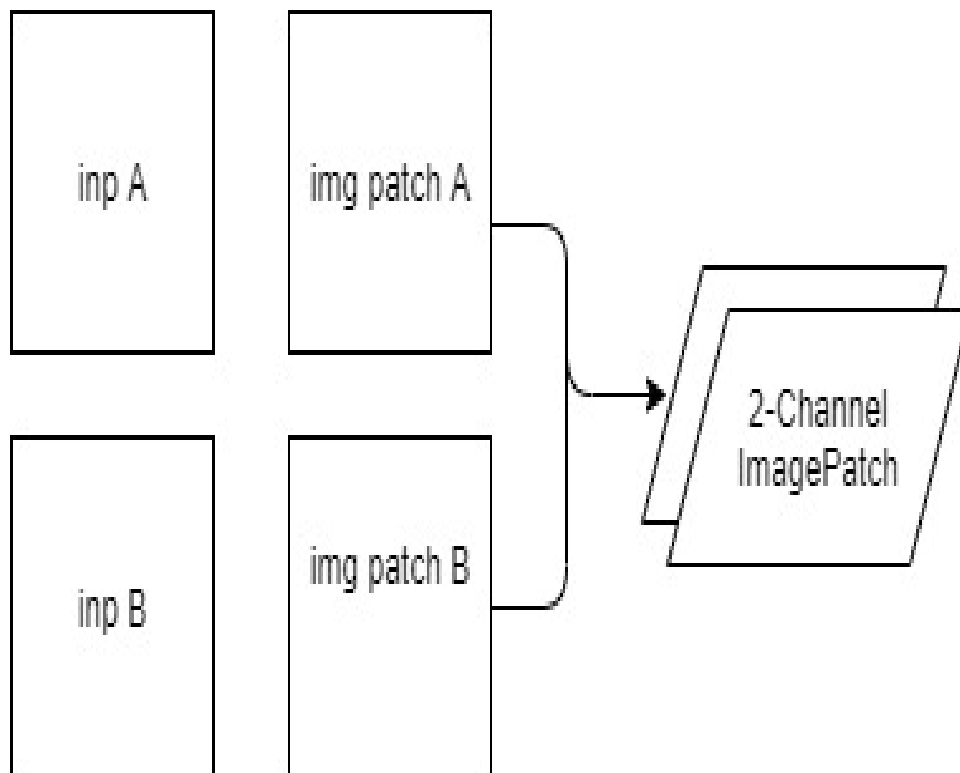
FIGURE 2.2: Image Fusion Using 2 Channel Input Images.

According to Ali et al [27] the blur finding and segmentation for a single image without any previous knowledge is a tricky task. They anticipated various methods for blur finding and segmenting to restore the sharp image. They offered the performance analysis of the state-of-the-art defocuses evaluated operators under a combined scaffold for defocus segmenting. Multiple evaluated operators are measured for relating to a varied set of actual defocus images pretended by various kinds of defocus levels and noise. Ali et al [27] presented minute changes in the defocus map categorization steps of this agenda and they have engaged the Interquartile Range (IQR) of the early defocus map for its categorization in

replacement of some permanent thresholds. They used 32 defocus measure operators to perform their analysis. The completion of the operators is measured by different qualitative measures. The conclusion shows that the defocus measure operators performed well under some situations and factors. Some operators performed satisfactorily and some did not.
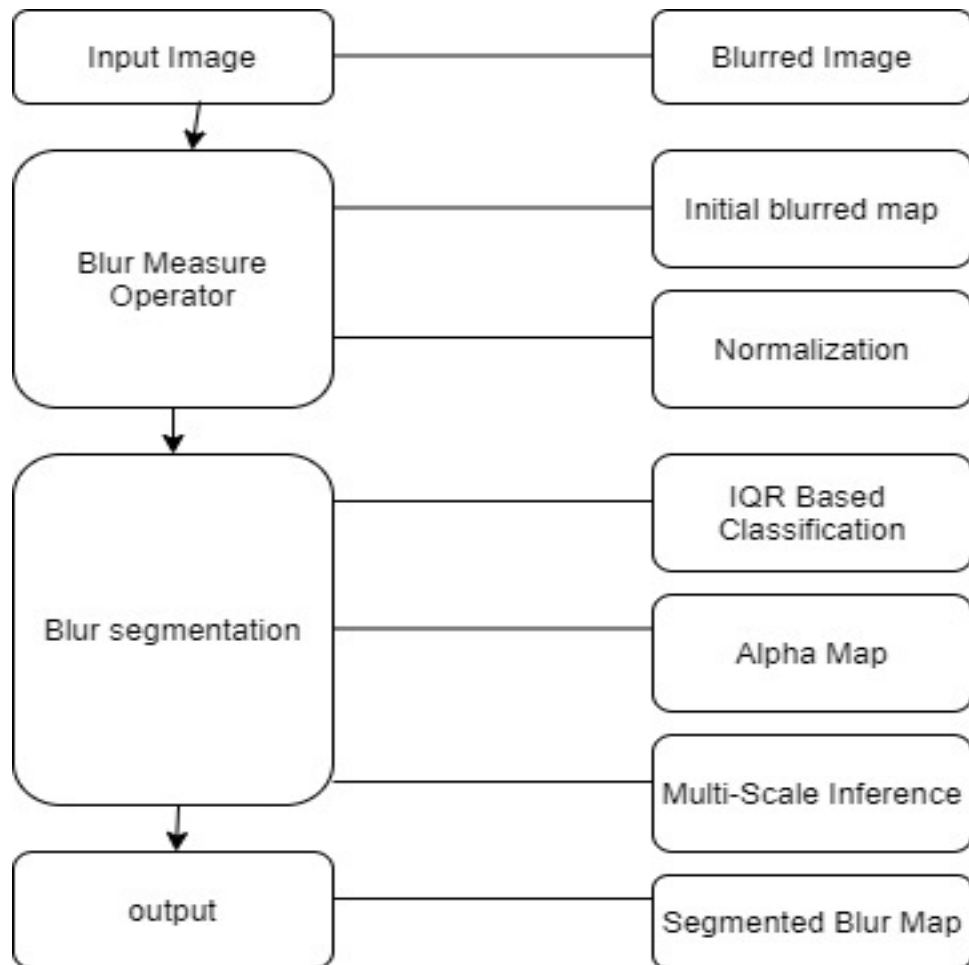
FIGURE 2.3: Framework for Blur Segmentation.

According to Ojala et al [28] the out-of-focus shade is frequent in an image capturing by using the optical imaging method. For the process of image restoration and object recognition segments, the incomplete blur image is converted into focus and defocus region. They [28, 29] proposed a sharpness metric dependent on LBP (local binary patterns) and a strict segmenting algorithm to focus apart and blur region of images. The projected sharpness metric showed that some image

parts in defocus regions have considerably lessened of some local binary patterns contemplated to those in-focus regions. The sharpness map is generated by image matting and multiscale inference. They experimented on hundreds of incompletely defocus images to compute the defocus segmenting algorithm and six methods for comparison. The consequences showed that the algorithm obtained proportional segmentation outcomes as compared to state-of-the-art techniques and have the benefit of high-speed over other techniques.

2.2 Critical Review

The results of different authors are compared based on the above questions and then results are computed. However, there are some concepts of multi-focus image fusion introduced by different authors but nobody has utilized the approach of LBP-map based image fusion.

TABLE 2.1: Literature Survey of Image Fusion

Ref	Methodology	Strength	Weakness
[4]	Novel optimized mixed spatial fusion	Eliminate Drawback of single spatial domain approach	Performance can be improved using variable block size
[18]	Discrete cosine transform (DCT) based standards in WVSN.	Better performance than old DCT techniques.	Perform only objective evaluation. Not subjective evaluation

[11]	Novel method proposed, which used the Sobel operator	Produce better entropy and mutual information value also improve the image quality index.	Image Contrast can be further improve
[12]	Super-resolution technique based on interpolation using (DWT)	DSAR provide a better result than the conventional image resolution enhancement	DASR can be improve by using more sophisticated interpolation techniques.
[13].	Artificial Bee Colony optimization algorithm (ABC).	Better performance then Laplacian pyramid and DWT.	Fixed block size
[16]	Region-Based Image fusion using Genetic Algorithm	Better perform then Haar wavelet approach and Morphological wavelet approach	Fixed block size
[15]	Multi-resolution signal decomposition scheme called Laplacian pyramid method.	Compute local and global information	Complexity and real-time are more improvable.
[19]	Residual networks method and 2-channel model	Generate decision map using post-processing and apply deep neural network.	Not used binarization method for post processing

[20]	Convolution neural network.	Overcome manual design and used activity level measurement.	Used fixed size threshold.
[21]	Combination of Multiscale Transform (MST) and Sparse Representation (SR)	Improve the algorithms strength to misregistration by 1-level disintegration. Faster than the SR method since the time consuming sparse coding method.	Guided filter is better then MST-SR for multi-focus image fusion.
[22]	Dense scale-invariant feature transform (SIFT)	Find decision map. refine the decision map.	Computational efficiency is lower than guided filtering. The memory requirement is high.
[23]	Sparse representation based multi-focus image fusion method.	Overcome image restoration and fusion problem by varying estimated measure.	Used only DCT base Dictionary instead of other techniques are available like learning base method
[8]	Novel multi-focus image fusion based on a random walk and guided filter	Fully utilized by regulating proportional coefficient artificially and good edge-preserving and smooth effect	Low mutual information

Chapter 3

Methadology

3.1 Blur Measure Operators

There are multiple types of blur measure operators that can be employed to estimate the classification of a pixel in an image as blurred or non-blurred. Based on this decision, all the pixels in an image can be selected to construct a blur segmented map. Different defocus measures provide different defocus measures for the identical pixels [27]. Lets consider a blurred input image $Img_b(i,j)$. The effect of blur on a pixel location $W(i,j)$ is calculated by applying to defocus measure operator BO based on its neighborhood using a kernel of multiple sizes such as 3x3 5x5, etc. The kernel is moved on each pixel one by one in an overlapping fashion and the whole image is traversed to generate a blur segmented map $BM(i,j)$.

$$BM(i,j) = BO(Img_b(i,j)) \tag{3.1}$$

The constructed blur segmented map is normalized to obtained a normalized blur segmented map using min and max measurements according to the Eq (3.2)

$$BM^{'}(i,j) = \frac{BM(i,j) - min(BM)}{max(BM) - min(BM)^{'}} \tag{3.2}$$

3.1.1 Types of Blur Measure Operators

Blur measure operators are divided into four Categories [27]. 1. Statistical-based operators. This type includes different statistical blur measures. These measures calculate the magnitude of blurriness on a pixel using its neighboring according to the kernel size. e.g Local binary pattern, Gray level variance and DCT energy ratio.

2. Derived based Operators. This type of blur measure is based on image derivative. The assumption about this derivative is that the edges in the non-blurred region of an image remain intact. The blurriness badly affects the detail present in an image. e.g Gaussian derivative, Gradient energy, and squared gradient.

3. Transform-based operators. In this type of blur operators, the measurement is dependent on the transform domain representation of the image content. Content of image frequency can be used to distinguish the focus and defocus region of the image e.g Power spectrum, a sum of wavelet coefficients, and variance of wavelet coefficients.

4. Miscellaneous Operators. These blur operators do not belongs to any above category. e.g image contrast and spatial frequency.

3.2 Process of LBP Measurements

LBP is a texture-based defocus measure operator which belongs to derived based measure operators. This operator given in Eq (3.7) allows uniform local binary patterns at any spatial resolution and in circular neighborhoods. Where T is a texture, x_c is a gray value of central pixels, and $x_p(p = 0, 1 - - - - - - Px - 1)$ indicates gray values of neighborhood pixels which are located on the equal distance at a circle of the radius where R is radius $R(R > 0)$ as shown in Figure3.1. If a gray value is not located at a central pixel, then this value can be estimated by the linear interpolation method.

If coordinate of x_c are (0,0) then coordinates of x_p are given by $(-R \sin[2\pi/Px]$, $(R \cos[2\pi/Px]$. The pixel value can be estimated by interpolation when a gray value of neighboring pixels is not located at a central pixel [28][29]. First of all gray value of the central pixel x_c is subtracted form the gray value of the neighboring pixels x_p with a minimal loss of information.

$$T = t(x_c, x_0 - x_c, x_1 - x_c, ...x_{Px-1} - x_c) \tag{3.3}$$

The obtained LBP codes can be stored in a p-dimensional histogram. When the input region is constant then outcomes of all directions is zero. The change in edges texture indicates high difference in all directions.

$$LBP_{Px,R} = \Sigma_{p=0}^{Px-1} S(x_p - x_c) * 2^p \tag{3.4}$$

$$S(x) = 1|x| >= T_{LBP}, 0|x| < T_{LBP} \tag{3.5}$$

The $LBP_{Px,R}$ is a unique number that characterizes a spatial structure of local image texture. The output of the $LBP_{Px,R}$ remains constant when the gray value of the image is the same. When Px=8 and R=1 then $LBP_{8,1}$ is obtained which is similar to the proposed LBP operator. The other term 2^p indicates gray level values differences which can be formed by Px pixel in a neighborhood pixel set. The gray value x_0 is always assigned to the right of the x_c, The x_p is located in a perimeter of a circle of x_c and return binary patterns. The unique identifier is assigned to each rotation invariant local binary patterns to remove the effects of rotation using Eq (3.6).

$$LBP_{Px,R}^{ri} = min(ROR(LBP_{Px,R}, i)|i = 0, 1, 2, 3.....Px - 1) \tag{3.6}$$

$$T = t(x_c, x_p, ...x_{Px-1}) \tag{3.7}$$

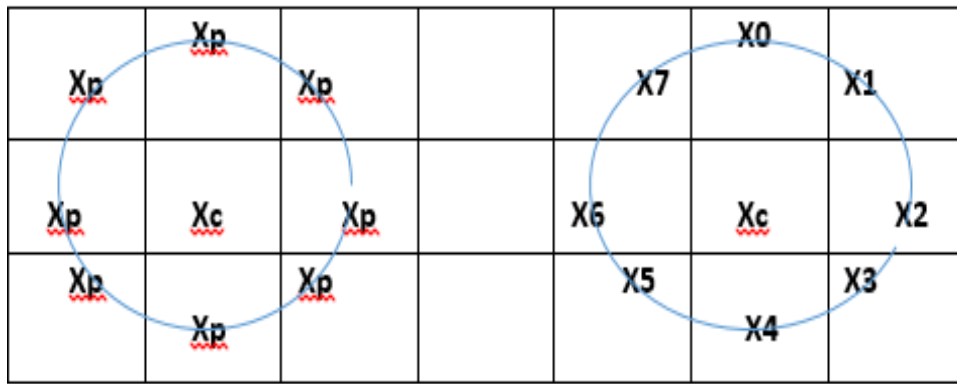There are two kind of pattern are created which are uniform pattern and non-uniform pattern.

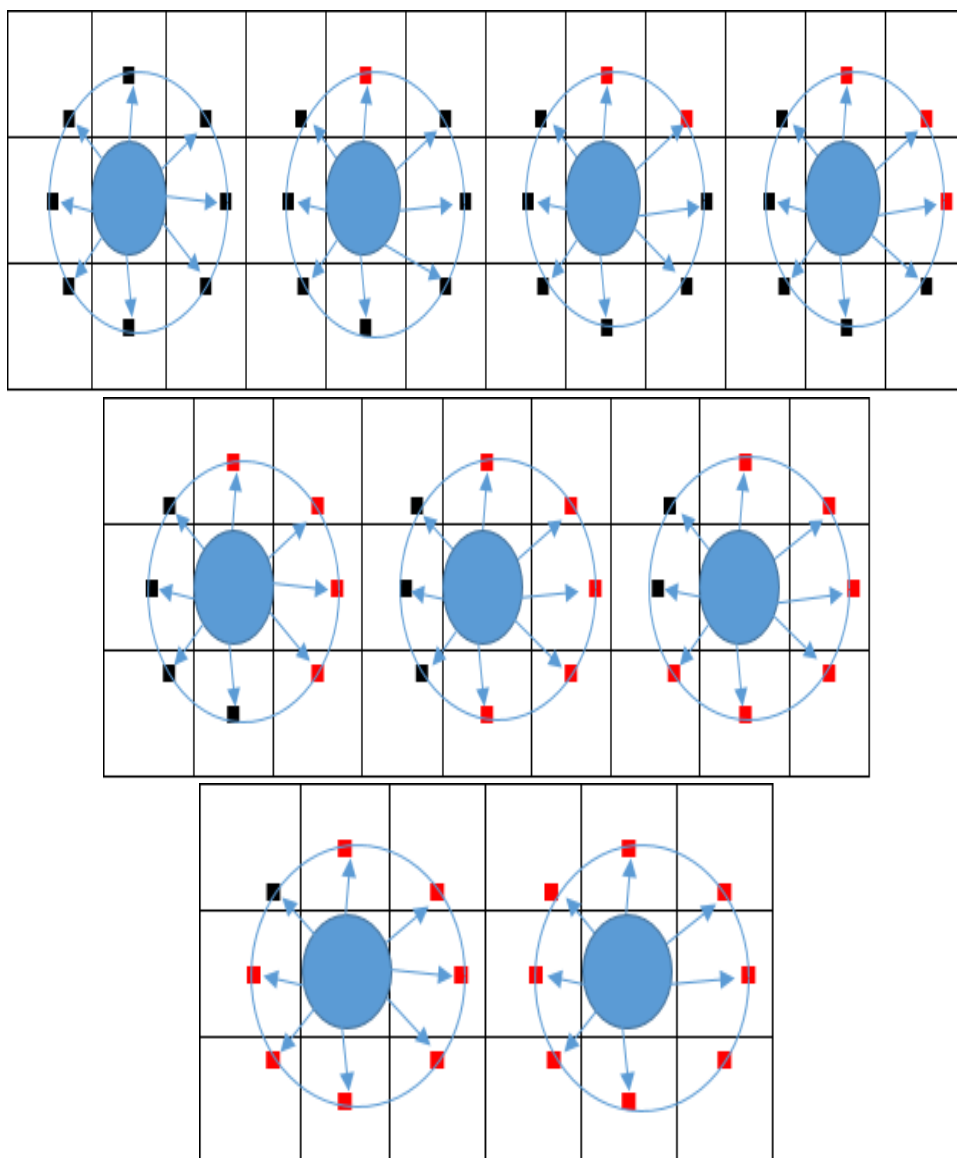FIGURE 3.1: LBP Based Rotation Invariant Blur Segmentation.

FIGURE 3.2: LBP based Rotation Invariant Steps for Blur Segmentation.

where $ROR(x, i)$ operator perform circular bit-wise right shift on the Px-bit number x,i times. The neighboring pixel set is rotating clockwise multiple times and obtain a most significant bit. The pattern can be used as a feature detector. When Px = 8 then the rotation invariant local binary pattern of $LBP_{8,1}$ is 36 [28]. These patterns contain different gray values like LBP Code 0 which contain all zero gray values which are a clear indicator of the full bright locality. The LBP code 1 to 7, each contains only two transitions like 0,1 and 1,0. The LBP code 8 contains all gray values one which shows a flat area and darker locality. The uniform pattern and finer quantization of angular space are used to improve the rotation invariance. Many uniform and non-uniform patterns are using Eq (3.9). Uniform patterns are those which contain at most 2 transitions of 0,1 or 1,0, while the pattern having more then 2 transitions are non-uniform patterns. The pattern 0 and 8 are uniform patterns because LBP code 0 contains zero U value 00000000_2 where all the gray value are zero and pattern 8 also contain zero U value 11111111_2 where all the gray values are one. The patterns 1 to 7 are also uniform because of only two transition 0 to 1 and 1 to 0. All the other patterns contain more than two U values so they are non-uniform patterns.

$$LBP_{Px,R}^{riu^2} = \Sigma_{p=0}^{Px-1} S(x_p - x_c) if U(LBP_{Px,R}) <= 2, (Px + 1, otherwise) \quad (3.8)$$

where,

$$U(LBP_{Px,R}) = |S(x_{Px-1} - x_c) - S(x_0 - x_c)| + |\Sigma_{p=1}^{Px-1} S(x_p - x_c) - S(x_{p-1} - x_c)|$$
$$(3.9)$$

if the intensity difference from the central pixel is less then T_{LBP} then the neighboring pixel colored blue otherwise colored red as shown in Figure:3.2. The frequency of pattern 6,7,8 and 9 in defocus regions is less than the focus regions. The neighboring pixel intensity is mostly similar to the X_c in flat areas.

$$O_{LBP} = 1/N\Sigma_{l=6}^{9} n(LBP_{8,1}^{riu^2}) \quad (3.10)$$

N is the total number of pixels in the selected area which is used to normalize the

metric so that O_{LBP} belong to 0-1 shown in Eq (3.10). The threshold T_{LBP} in Eq (3.5) controls the metirc sensitivity to sharpness. When T_{LBP} is increasing, then the metric become less sensitive to sharpness.

3.3 LBP-Map Based Fusion

To process raised issues of image fusions, the procedure mentioned in figure Figure3.5 is selected. The proposed methodology contains multiple steps such as dataset gathering, image segmentation using LBP sharpness metric, image fusion, objective and visual evaluation of output fused image.

3.3.1 Image Segmentation using LBP Sharpness Metric

The source images can be segmented into a focus and non-focus regions by using an LBP-based sharpness metric. First of all, the LBP-sharpness of each source image of the same scene is calculated separately. LBP-sharpness algorithm follows four important steps such as multi-scale sharpness map computation, alpha matting initialization, alpha map generation and multi-scale sharpness inference shows in figure 3.3. [29].
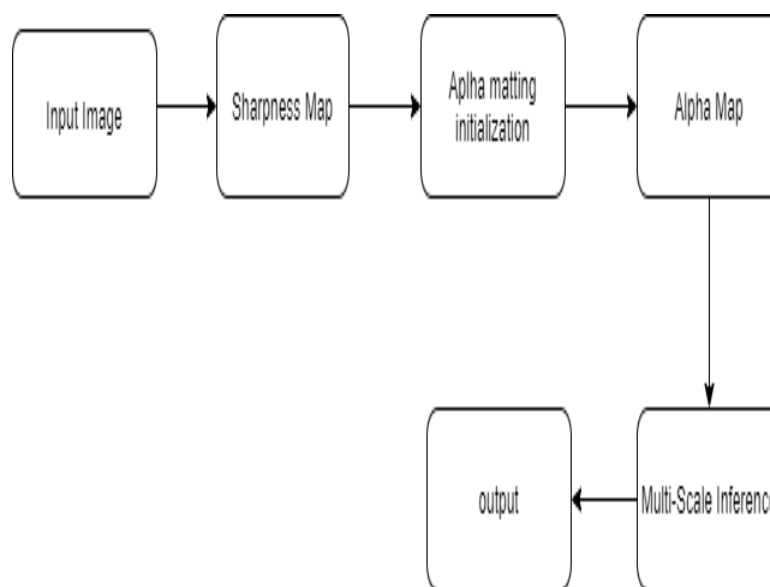
FIGURE 3.3: Blur Segmentation Steps.

3.3.1.1 Multi-scale Sharpness Map Computation.

The first step of LBP-sharpness metric is Multi-scale map computation. In this step, the algorithm M_{LBP} generates multi-scale sharpness maps using a local patch of 3x3, 5x5 and 7x7.

For local patch, sharpness metric is computed at each pixel of image[29]. The constant time per pixel for a fixed Px and R are calculate by sharpness maps.

3.3.1.2 Alpha Matting Initialization

It is a technique which is used to divide an image into foreground and background regions using Eq (3.11):

$$Img(i,j) = \alpha_{(i,j)}F(i,j) + (1 - \alpha_{(i,j)})B(i,j) \tag{3.11}$$

where the alpha mate, $\alpha_{i,j}$, refers significance of pixel location (i,j) which can be taken as the assurance of the foreground pixels.

When, taking foreground as focus and background as defocus, then alpha matting process is modified automatically. In this process, double threshold are used to compute the sharpness maps of initial value of α for each pixel using Eq (3.12) [28][29]:

$$Mask^s(i,j) = [1, if M_{LBP}(i,j) > T_{m1}].[0, if M_{LBP}(i,j) < T_{m1}].[M_{LBP}(i,j), otherwise]. \tag{3.12}$$

where s indexes the scale, that is, $Mask^s(i,j)$ is the initial $\alpha - map$ at the s-th scale.

3.3.1.3 Alpha Map Generation

The $\alpha - map$ can be computed by minimizing a cost function in Eq (3.13)[29].

$$E(\alpha) = \alpha(TL)\alpha + \lambda(\alpha - \alpha')T(\alpha - \alpha') \tag{3.13}$$

According to the above equation if α is a vector $\alpha - map$ and $\alpha' = Mask^i(i,j)$ are the alpha maps of vector initialization.

The L is a Laplacian matrix of matting which ensures regulation and encourages similarity to α' [29]. The alpha matting is applied at each scale which shows output alpha map α_s where s = 1, 2, 3.

This process is used to generate the alpha map of the image for fusion prupose.

3.3.1.4 Multi-scale Inference

When alpha map is computed at each scale, then multi-scale graphical model are produced.

This process is used to calculate the total energy of the model using Eq (3.14).

$$E(y) = \Sigma_{s=1}^3 \Sigma_i |y_i^s - y_i'^s| + B(\Sigma_{s=1}^3 \Sigma_i \Sigma_{j=N_i^s}^3 |y_i^s - y_i'^s| + \Sigma_{s=1}^2 \Sigma_i |y_i^s - y_i^{s+1}|) \quad (3.14)$$

where $y_i'^s = \alpha_i^s$ is the alpha map at pixel position i and y_i^s is the sharpness. The assigning sharpness value y_i^s are the cost.

The output of the algorithm h^3 is the sharpness map at the largest scale where high intensity indicates high sharpness[28, 29].

3.4 Input Images Dataset

To evaluate this proposed methodology, a dataset is required which must contain multi-focus images of relevant scene or activity. A total of twenty five multi-focus pair of images are collected from a renowned lytro image dataset [30]. In this dataset, each pair of images contains a set of two images. This dataset contain background focus and foreground focus image This dataset also contain some right focus and left focus images.

If blurriness of an image is high its means de-focus part is greater then the focus part and if non-blur part of an image is high then focus part is greater then the de-focus part. These images are visually illustrated in figure 3.1 below.
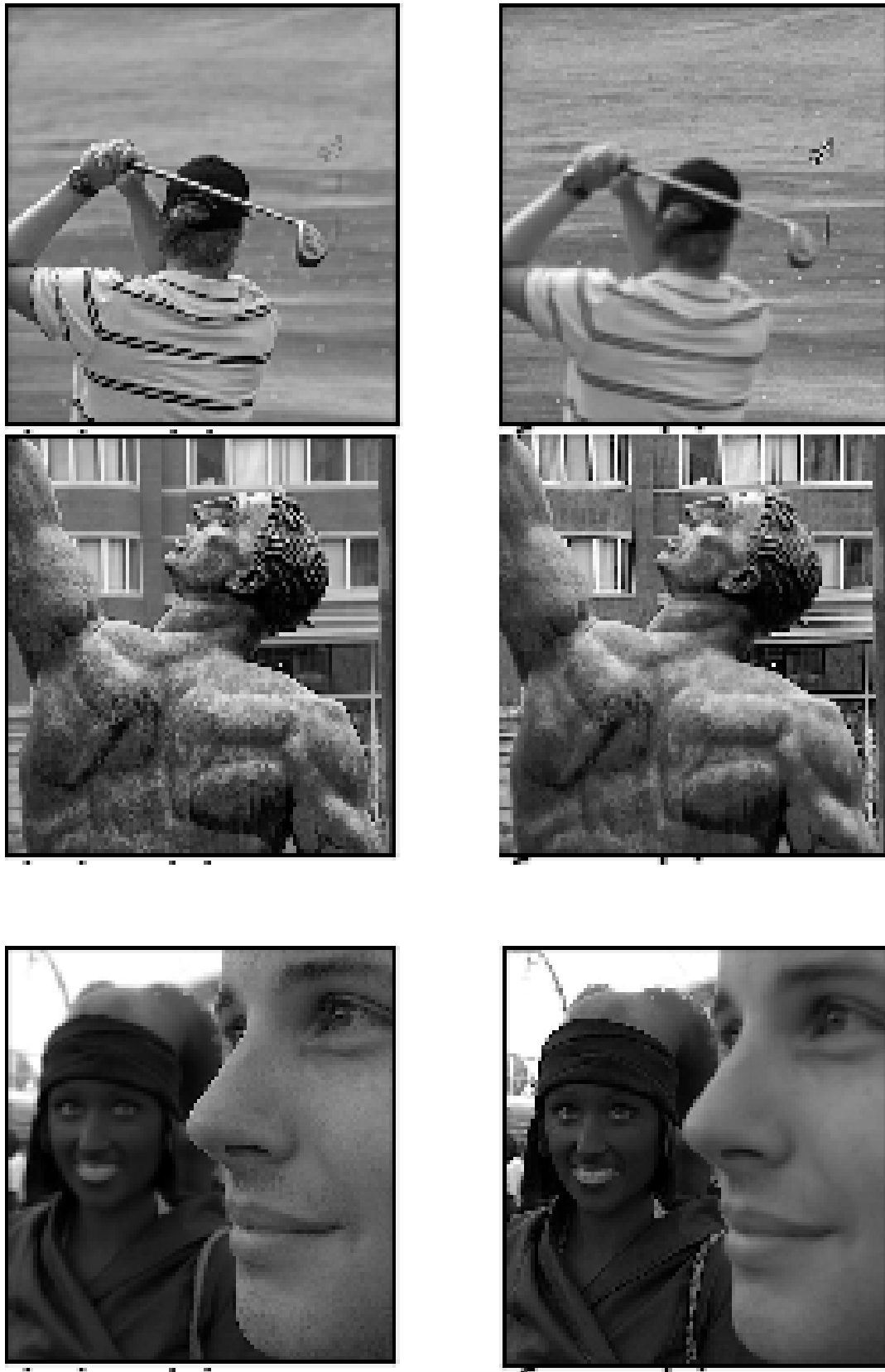
FIGURE 3.4: Visual Illustration of Multi-focus Image Dataset.

Algorithm 1 LBP Based Image fusion

1: **procedure** –

2:      Input:$Img_a(i,j)$ local patch size of 3x3.

3:      Output:Uniform LBP image $map_{LBP}(i,j)$

4:      Read the input image as $Img_a(i,j)$

5:      **for** each node $k \in i$ **do**

6:        **for** each node $l \in j$ **do**

7:          Apply an overlapping kernal, with a block size of 3x3.

8:          Take the first image block of 3x3 along with its pixel intensities.

9:          Take the intensity of a central pixel as a threshold T in that particular kernal.

10:          Compare the intensities of neighboring pixels with T.

11:          **if** $P_x(i,j) >= T$ **then**

12:            return 1

13:          **else if** $P_x(i,j) < T$ **then**

14:            return 0

15:          **end if**

16:          Return an 8-bit binary code.

17:          Convert 8-bit binary code into decimal

18:          Replace the value of central pixel, with obtained decimal value.

19:        **end for**

20:      **end for**

21:      Until: the image is not completely compared.

22:      Compare all binary codes.

23:      NO pattern contain more than two transition 01

24:      Collect all noisy entries in a separate bin in a particular histogram.

25:      return:Uniform LBP image $map_{LBP}(i,j)$

26: **end procedure**

3.4.1 Fussion Process

LBP segmentation algorithm are tested by using aforementioned dataset which contains 20 partially blurred images. First of all, LBP-sharpness algorithm are used to extract an LBP-map. Later, this process creates iamge segmentation using LBP map and then fusion is applied. In the process of fusion, a fused image is genrated by comparing each pixels of segmented images one by one. If pixel of segmented image one with high intensity gray value and pixel one of segmented image two with low intensity gray value then pixel one from input image one is placed in a new image and vice verse. On comparison completion, this process returns an all in focus output fused image. The complete process of proposed methodology are shown in figure 3.5.

Algorithm 2 LBP Based Image fusion

procedure –

2:       Input:$Img_a(i,j)$ and $Img_b(i,j)$ local patch size of 3x3.

      Output:Fused image $Img_F(i,j)$

4:       Calculate LBP sharpness as $O_{LBP1}(i,j)$

      Calculate LBP sharpness as $O_{LBP2}(i,j)$.

6:       **for** each node $k \in i$ **do**

          for each node $l \in j$ **do**

8:               **if** $map(k,l) = 1$ **then**

                $Img_F(i,j) = Img_a(i,j)$

10:               **else if** $map(k,l) = map(k,l)$ **then**

                $Img_F(i,j) = Img_a(i,j)$

12:               **else**

                $Img_F(i,j)= Img_a(i,j)$

14:               **end if**

          end for

16:       **end for**

      return: $Img_F(i,j)$

18: **end procedure**
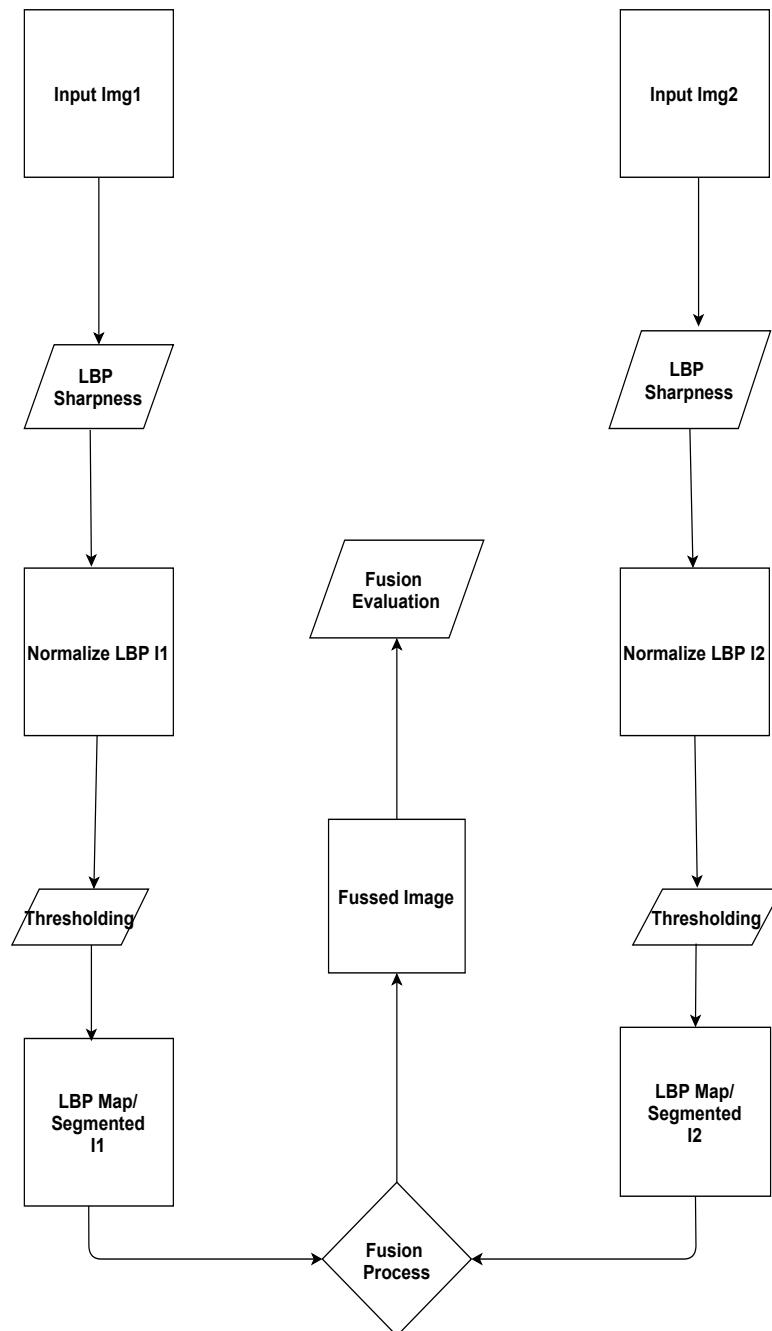
FIGURE 3.5: Methodology Diagram of Image Fusion.

3.5   Quality Metric

To measure the objective and subjective analysis of fused image, four different quality metric are employed. Our selected metrics are gradient metric, chen blum, yang metric and mutual information.

3.5.1   Gradient Metric.

For the calculation of gradient metric first of all the angle and magnitude of the input images A , B and F is calculated using Eq (3.15)-(3.20) equations [31][32][33].

$$\alpha_A(i,j) = \tan^{-1} \frac{S_A^x(i,j)}{S_A^y(i,j)} \tag{3.15}$$

$$\alpha_B(i,j) = \tan^{-1} \frac{S_B^x(i,j)}{S_B^y(i,j)} \tag{3.16}$$

$$\alpha_F(i,j) = \tan^{-1} \frac{S_F^x(i,j)}{S_F^y(i,j)} \tag{3.17}$$

$$G_A(i,j) = \sqrt{S_A^x(i,j)^2 + S_A^y(i,j)^2} \tag{3.18}$$

$$G_B(i,j) = \sqrt{S_B^x(i,j)^2 + S_B^y(i,j)^2} \tag{3.19}$$

$$G_F(i,j) = \sqrt{S_F^x(i,j)^2 + S_F^y(i,j)^2} \tag{3.20}$$

Here we notice that $S_A^x(i,j)$ and $S_A^y(i,j)$ are the vertical and horizontal sobel operator at location(i,j) of image A while $S_B^x(i,j)$ and $S_B^y(i,j)$ are vertical and horizontal sobel operator at location(i,j) of image B.

For fused image vertical and horzontal sobel operator are calculated by $S_F^x(i,j)$ and $S_F^y(i,j)$. F is an fused image and A,B are the source input images. Now compute the $G_A(i,j)$, $G_B(i,j)$ and $G_F(i,j)$ [34][35].

$$\Delta^{AF} = 1 - \frac{\alpha_A(i,j) - \alpha_F(i,j)}{\pi/2} \tag{3.21}$$

$$\Delta^{BF} = 1 - \frac{\alpha_B(i,j) - \alpha_F(i,j)}{\pi/2} \tag{3.22}$$

if $G_A(i,j) > G_F(i,j)$ then $G^{AF}(i,j)$ is calculated as $\frac{G_F(i,j)}{G_A(i,j)}$ otherwise $G^{AF}(i,j)$ is calculated as $\frac{G_F(i,j)}{G_A(i,j)}$. Now calculate the $G^{AF}(i,j)$ and $G^{BF}(i,j)$.

$$G^{AF}(i,j) = \frac{G_F(i,j)}{G_A(i,j)} G_A(i,j) > G_F(i,j) OR \frac{G_F(i,j)}{G_A(i,j)} Otherwise \tag{3.23}$$

$$G^{BF}(i,j) = \frac{G_F(i,j)}{G_B(i,j)} G_B(i,j) > G_F(i,j) OR \frac{G_F(i,j)}{G_B(i,j)} Otherwise \tag{3.24}$$

Here is some constant values for the calculation of below equations. The constant values are T_g=1,K_g=-10,σ_g=0.5, T_α=1,K_α=-20,σ_α=0.75

$$Q_\alpha^{AF}(i,j) = \frac{T_\alpha}{1 - e_\alpha^K(\Delta^{AF}(i,j) - \sigma_\alpha)} \tag{3.25}$$

$$Q_\alpha^{BF}(i,j) = \frac{T_\alpha}{1 - e_\alpha^K(\Delta^{BF}(i,j) - \sigma_\alpha)} \tag{3.26}$$

$$Q_g^{AF}(i,j) = \frac{T_g}{1 - e_g^K(G^{AF}(i,j) - \sigma_g)} \tag{3.27}$$

$$Q_g^{BF}(i,j) = \frac{T_g}{1 - e_g^K(G^{BF}(i,j) - \sigma_g)} \tag{3.28}$$

Now calculate the $Q_\alpha^{AF}(i,j)$, $Q_\alpha^{BF}(i,j)$ and $Q_g^{AF}(i,j)$, $Q_g^{BF}(i,j)$ using Eq (3.25)-(3.28). This can be calculate the sobel edge strength and orientation preservation value.

$$Z^{AF}(i,j) = Q_g^{AF}(i,j)Q_\alpha^{BF}(i,j) \tag{3.29}$$

$$Z^{BF}(i,j) = Q_g^{BF}(i,j)Q_\alpha^{AF}(i,j) \tag{3.30}$$

Finally the ***gradient of the image*** is calculated which contain source image A , source image B and fused image F.

Now calculate the $Z^{AF}(i,j)$ and $Z^{BF}(i,j)$ and also calculate the $W_a(i,j)$ and $W_b(i,j)$ which are two weights of $Z^{AF}(i,j)$ and $Z^{BF}(i,j)$.

$$W_a(i,j) = |Z^{AF}(i,j)| \tag{3.31}$$

$$W_b(i,j) = |Z^{BF}(i,j)| \tag{3.32}$$

$$Q_{grad} = \frac{\sum_{n=1}^{N} \sum_{m=1}^{M} Z^{AF}(i,j)W_a(i,j) + Z^{BF}(i,j)W_b(i,j)}{\sum_{n=1}^{N} \sum_{m=1}^{M} W_a(i,j) + W_b(i,j)} \tag{3.33}$$

3.5.2   Chen Blum

Chen blum is based on human perception fusion metric. They used important feature in the human visual system model[36][34].

3.5.2.1   Contrast Sensitivity Filtering

Let us consider $T_A(m,n)$ define the Fourier Transform of the original input image $Im_A(i,j)$ where (i,j) is the pixel location

$$T'_A(m,n) = T_A(m,n)S(d) \tag{3.34}$$

where S(d) is CSF in polar coordinates $d = \sqrt{m^2 + n^2}$.

The inverse Fourier Transform is applied to the filtered response $T_A(m,n)$, $T_B(m,n)$ and $T_F(m,n)$ to yield $I_A(x,y)$, $I_B(x,y)$ and $I_F(x,y)$.

Lets calculate the local contrast computation using local RMS contrast which can define a round kernel of radius rad containing N pixels.

Weights are assign to the i_{th} pixel in the window[36].

$$w_i = 0.5(\cos(\pi/rad\sqrt{(i_x - i)^2 + (j_y - j)^2}) + 1) \tag{3.35}$$

$I' = \Sigma_{i=1}^{N} w_i I_i$ and local contrast function of source image I

$$Cn^{rms}(i,j) = \left(\sqrt{\frac{1}{\Sigma_{x=1}^{N} w_i} \Sigma_{x=1}^{N} w_i \frac{(I_x - I')^2}{I' + I_d}}\right) \tag{3.36}$$

I_d is the "dark light" parameter chosen to be $1cd/m^2$.

3.5.2.2 Preservation Calculation of Contrast

The amount of information are calculated from input image and transform it into I_A.

If input image A are taken for calculation of contrast map of Cn_A and vice verse [36].

$$Cn_A' = \frac{E(Cn_A)^p}{F(Cn_A)^q + U} \tag{3.37}$$

for image B and fused image.

$$Cn_B' = \frac{E(Cn_B)^s}{F(Cn_B)^t + U} \tag{3.38}$$

where E, F, Z,s and t are the scalar parameters which can shows the shape of the non-linear mask function.

$$G^{AF}(i,j) = \frac{Cn_A'(i,j)}{Cn_F'(i,j)} if Cn_A'(i,j) < Cn_F'(i,j) OR \frac{Cn_F'(i,j)}{Cn_A'(i,j)} Otherwise \tag{3.39}$$

$$G^{BF}(i,j) = \frac{Cn_B'(i,j)}{Cn_F'(i,j)} if Cn_B'(i,j) < Cn_F'(i,j) OR \frac{Cn_F'(i,j)}{Cn_B'(i,j)} Otherwise \tag{3.40}$$

The range of value of $G_{AF}(i,j)$ is between [0,1]. $G_{AF}(i,j) = 1$ its mean information preserved form input image A to fused image F without any loss of information. $G_{AF}(i,j) = 0$ its meant complete loss of information.

If the loss of information is minimum the result of fusion image is increased. If loss of information is maximum the result of fused image is decreased.

3.5.2.3 Saliency Map Generation

For identification of visual saliency on the base of human observer used as a masked contrast map. λ_A is the saliency map of input image A [36].

$$\lambda_A(i,j) = \frac{Cn_A^{'2}(i,j)}{Cn_A^{'2}(i,j) + Cn_B^{'2}(i,j)} \tag{3.41}$$

Saliency map for image B is computed as

$$\lambda_B(i,j) = \frac{Cn_B^{'2}(i,j)}{Cn_A^{'2}(i,j) + Cn_B^{'2}(i,j)} \tag{3.42}$$

3.5.2.4 Global Quality Map

The global quality map is computed as

$$Q_{Cn}(i,j) = \lambda_A(i,j)G^{AF}(i,j) + \lambda_B(i,j)G^{BF}(i,j) \tag{3.43}$$

Every value of the final output is between 0 and 1.

For obtaining the single value of the final map the mean are calculate for every pixels.

$$Q_z = Q_{Cn} \tag{3.44}$$

3.5.3 Mutual Information

The measurement of relative independence of couple of images which used multi-model image registration.

If high value is obtained its mean point-out the highly dependence [34][33].

$$MI(i,j) = E(i) + E(j) - E(i,j) \tag{3.45}$$

E denote the entropy E(i,j) is the joint entropy which can compute the joint density of two source image i and j.

$$NMI(i,j) = \frac{E(i) + E(j)}{2E(i,j)} \tag{3.46}$$

By using the above equation quality map of fused image is compute [10].

3.5.4 Yangs Fusion Metric.

Yang metric is based on the structural similarity index measure which can measure the structural information of the input image [37][35].

$$Q_y = T(w)SSIM(A,F|w) + (1 - T(w))SSIM(A,F|w), T(w)SSIM(A,B|w) > 0.075 \tag{3.47}$$

$$Q_y = maxSSIM(A,F|w), SSIM(A,F|w), T(w)SSIM(A,B|w), 0.075 \tag{3.48}$$

W is the kernel size and T(w) is the local weight of kernel.

$$T(w) = \frac{a(Aw)}{a(Aw) + s(Bw)} \tag{3.49}$$

Chapter 4

Experiment and Results

4.1 Experiments

In this chapter, the results of image fusion using LBP sharpness blur measure are discussed and presented. Many experiments are performed for extracting and analyzing performance of blur measure operator. The segmented image shows clear distinctive response using selected suitable blur measure operator. Focus and defocus part are clearly differentiated from decion map of the input images.

4.1.1 Objective Evaluation of Fused Images

Multiple experiments are presented using different thresholds on multi-focus images of lytro image dataset[30]. The threshold values can be changed for computing better results. If small value of threshold is used then a better performance is achieved. The window size 3x3 are used for this experimentation. The selection of small threshold with small kernal size provide efficient results of quality metrics. The four quality metrics are employed such as 1) Normalize mutual information, 2) gradient metric, 3) yang metric and 4) chen-blum. The selected thresholds for results are 0.0005, 0.0002, 0.0001, 0.000075, 0.00005, 0.00002.

Gray-scale I1   Gray-scale I2

Figure(A)   Figure(B)

Figure(C)   Figure(D)

Figure(E)   Figure(F)

Figure(G)   Figure(H)

Threshold Segmented I1   Segmented I2   Fused Image

0.0002

Figure(1A)   Figure(1B)   Figure(1C)

0.0002

Figure(1D)   Figure(1E)   Figure(1F)

0.0002

Figure(1G)   Figure(1H)   Figure(1I)

0.0002

Figure(1J)   Figure(1K)   Figure(1L)

Threshold	Segmented I1	Segmented I2	Fused Image

0.0001

Figure(2A)   Figure(2B)   Figure(2C)

0.0001

Figure(2D)   Figure(2E)   Figure(2F)

0.0001

Figure(2G)   Figure(2H)   Figure(2I)

0.0001
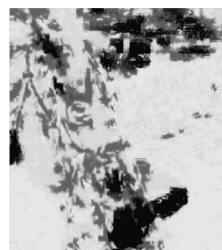
Figure(2J)   Figure(2K)   Figure(2L)

Threshold Segmented I1   Segmented I2   Fused Image

0.00002

Figure(3A)   Figure(3B)   Figure(3C)

0.00002

Figure(3D)   Figure(3E)   Figure(3F)

0.00002

Figure(3G)   Figure(3H)   Figure(3I)

0.00002

Figure(3J)   Figure(3K)   Figure(3L)

Threshold Segmented I1   Segmented I2   Fused Image

0.00005

Figure(4A)   Figure(4B)   Figure(4C)

0.00005

Figure(4D)   Figure(4E)   Figure(4F)

0.00005

Figure(4G)   Figure(4H)   Figure(4I)

0.00005

Figure(4J)   Figure(4K)   Figure(4L)

Threshold	Segmented I1	Segmented I2	Fused Image

0.0005

Figure(5A)   Figure(5B)   Figure(5C)

0.0005

Figure(5D)   Figure(5E)   Figure(5F)


0.0005

Figure(5G)   Figure(5H)   Figure(5I)

0.0005

Figure(5J)   Figure(5K)   Figure(5L)

Threshold Segmented I1   Segmented I2   Fused Image

0.00007

Figure(6A)   Figure(6B)   Figure(6C)

0.00007

Figure(6D)   Figure(6E)   Figure(6F)

0.00007

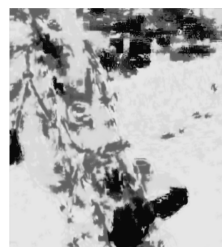Figure(6G)   Figure(6H)   Figure(6I)

0.00007

Figure(6J)   Figure(6K)   Figure(6L)

The fusion is applied on the basis of segmented images. The segmentation of images are perform using different thresholds. The Figure(A) is the segmented image of Gray-scale I1 and Figure(B) is the segmented image of Gray-scale I2. The four different datasets are used for this experimentation. This experimentation indicates the segmented images and finally fused the two Gray-scale images on the basis of segmented images. The experiment perform on the basis of thresholds. When threshold value = 0.0002, the qulity metrics of Figure(1C) is NMI=1.1731, Qy=0.9560, Qg= 0.7066 and CB=0.7942. The qulity metrics of Figure(1F) is NMI=1.1621, Qy=0.9410, Qg= 0.6816 and CB=0.7481. the qulity metrics of Figure(1I) is NMI=1.1811, Qy=0.9630, Qg= 0.7136 and CB=0.7882. The qulity metrics of Figure(1L) is NMI=1.2439, Qy=0.9620, Qg= 0.7366 and CB=0.8012.

When threshold value = 0.00002, the qulity metrics of Figure(3C) is NMI=1.2162, Qy=0.9663, Qg= 0.7346 and CB=0.8122. The qulity metrics of Figure(3F) is NMI=1.1930, Qy=0.9869, Qg= 0.7215 and CB=0.7916. The qulity metrics of Figure(3I) is NMI=1.1711, Qy=0.9634, Qg= 0.7330 and CB=0.7842. The qulity metrics of Figure(3L) is NMI=1.2154, Qy=0.9596, Qg= 0.7153 and CB=0.7965.

When threshold value = 0.00007, the qulity metrics of Figure(6C) is NMI=1.2019, Qy=0.9618, Qg= 0.7222 and CB=0.8072. The qulity metrics of Figure(6F) is NMI=1.1851, Qy=0.9772, Qg= 0.7246 and CB=0.7986. The qulity metrics of Figure(6I) is NMI=1.1915, Qy=0.9732, Qg= 0.6944 and CB=0.7945. The qulity metrics of Figure(6L) is NMI=1.2168, Qy=0.9641, Qg= 0.7053 and CB=0.7513.

The obtained value of quality metrics in Figure(3C) and Figure(3F) is high as compared with others thresholds. The obtained value of quality metrics in Figure(6I) is high as compared with others thresholds. The obtained value of quality metrics in Figure(1L) is high as compared with others thresholds.

The focus and defocus regions are increased due to change in thresholds. The presented technique is compared with 6 other techniques of image fusion. The previous techniques are sparse representation (SR), Non-subsampled contourlet transform sparse representation (NSCT-SR), Guided Filter (GF), Dense scale invariant feature transform (DSIFT) , Convolution Neural Network (CNN), Deep

Neural Network (DNN). The presented technique performed well as compare to these previous techniques.

According to Table 4.1 and Figure4.1 experimentation are perform on the basis of four quality metrics which are Normalize mutual information, Yang metric, chen Blum metric and gradient. The experimentation are based on six thresholds used for obtaining the results. LBP sharpness image is normalized image which contain all the values between 0 to 1. In LBP map or segmented image, zero indicate defocus area and 1 indicate focus area of the image.

The values of LBP sharpness image is below the threshold indicate the defocus region and greater values of threshold are fall in focus region. Therefore, small value of threshold indicating the maximum focus region of image while large value of threshold indicating the minimum focus or large defocus region.

TABLE 4.1: Results of LBP based Fusion Using Different Thresholds.

Threshold	NMI	Yang	ChenBlum	Gradient
0.0005	1.2028	0.9678	0.7726	0.6819
0.0002	1.2028	0.9723	0.7829	0.7031
0.0001	1.2029	0.9739	0.7865	0.7168
0.000075	1.2029	0.9769	0.8012	0.7208
0.00005	1.2029	0.9821	0.8024	0.7227
0.00002	**1.2030**	**0.9873**	**0.8050**	**0.7272**

FIGURE 4.1: Graph of Different Threshold.

In this experiment, proposed technique given in Table 4.2 and Figure4.2 are compared with other previous techniques. The previous techniques are sparse representation (SR) [38], Non-subsampled contourlet transform sparse representation (NSCT-SR) [21], Guided Filter (GF) [26], Dense scale invariant feature transform (DSIFT) [22] , Convolution Neural Network (CNN) [20] and Deep Neural Network (DNN) [19].

The threshold 0.0005 provides large non-focus area in segmented images. Therefore, results obtained using aforementioned threshold 0.0005 are lower as compared with previous techniques. A threshold is responsible for enhancing image sharpness.When threshold increases it becomes less significant to sharpness.

TABLE 4.2: Results of Previous Techniques and Proposed Technique where Threshold=0.0005.

Metrics	SR[38]	NSCT-SR[21]	GF[26]	DSIFT[22]	CNN[20]	DNN[19]	Proposed
NMI	1.0807	0.9651	1.1001	1.1902	1.1561	1.2002	**1.2028**
QG	0.6944	0.6823	0.7104	0.7162	0.7155	**0.7188**	0.6819
Qy	0.9663	0.9578	0.9775	0.9841	0.9851	**0.9871**	0.9678
QCB	0.7641	0.7499	0.7848	0.8005	0.8000	**0.8042**	0.7726
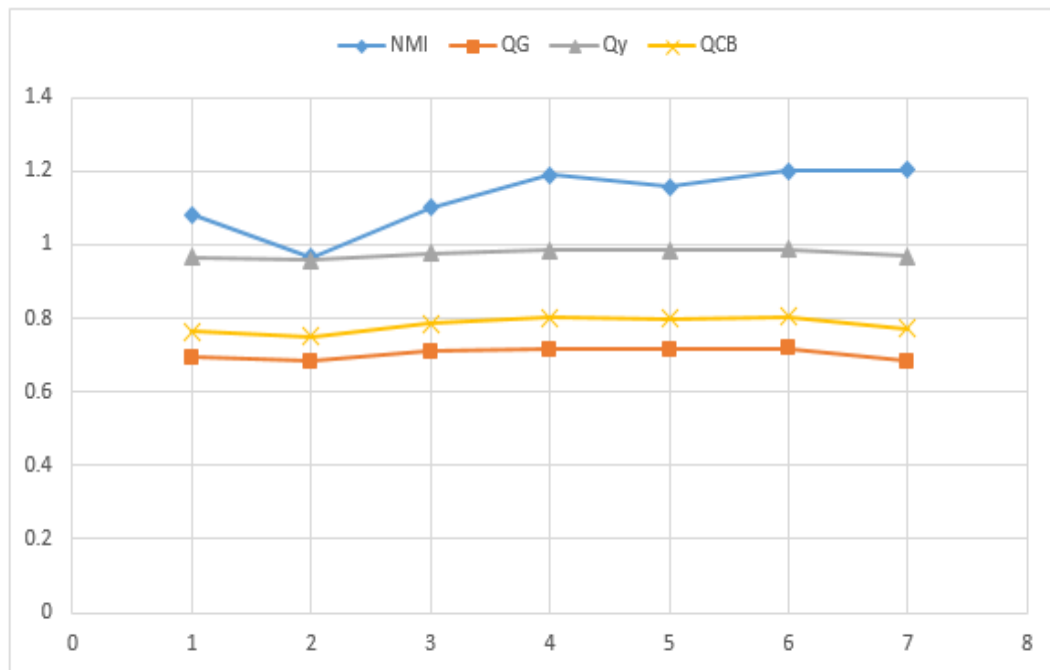
FIGURE 4.2: Graph of Previous Techniques and Proposed Technique where Threshold=0.0005.

The results obtained in Table 4.2 are lower as compared with previous techniques. In this experiment, The threshold 0.0002 is used which also provides less significant results and increases ringing artifacts in fused images.The threshold 0.0002 obtained better results as compare to the 0.0005 because it provides a higher number of focus region.The threshold 0.0002 also provides non significant results as compare to previous techniques.

TABLE 4.3: Results of Previous Techniques and Proposed Technique where Threshold=0.0002.

| Metrics	SR[38]	NSCT-SR[21]	GF[26]	DSIFT[22]	CNN[20]	DNN[19]	Proposed
NMI	1.0807	0.9651	1.1001	1.1902	1.1561	1.2002	**1.2028**
QG	0.6944	0.6823	0.7104	0.7162	0.7155	**0.7188**	0.7031
Qy	0.9663	0.9578	0.9775	0.9841	0.9851	**0.9871**	0.9723
QCB	0.7641	0.7499	0.7848	0.8005	0.8000	**0.8042**	0.7829

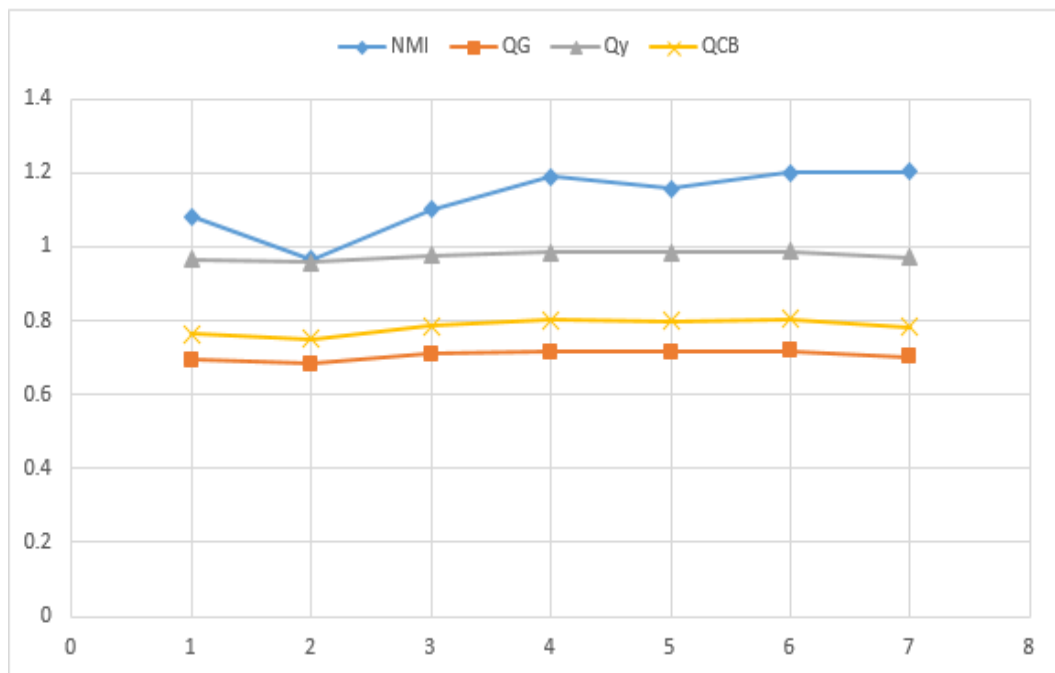FIGURE 4.3: Graph of Previous Techniques and Proposed Technique where Threshold=0.0002.

The results shown in Table 4.4 is better than the resluts of Table 4.2 and Table 4.3. The threshold 0.0001 obtained better results as compare to the 0.0005 and 0.0002 because its focus regions are more than the previous thresholds. The threshold 0.0001 also provides less significant results as compared with the previous techniques.

TABLE 4.4: Results of Previous Techniques and Proposed Technique where Threshold=0.0001.

Metrics	SR[38]	NSCT-SR[21]	GF[26]	DSIFT[22]	CNN[20]	DNN[19]	Proposed
NMI	1.0807	0.9651	1.1001	1.1902	1.1561	1.2002	**1.2029**
QG	0.6944	0.6823	0.7104	0.7162	0.7155	**0.7188**	0.7168
Qy	0.9663	0.9578	0.9775	0.9841	0.9851	**0.9871**	0.9739
QCB	0.7641	0.7499	0.7848	0.8005	0.8000	**0.8042**	0.7865

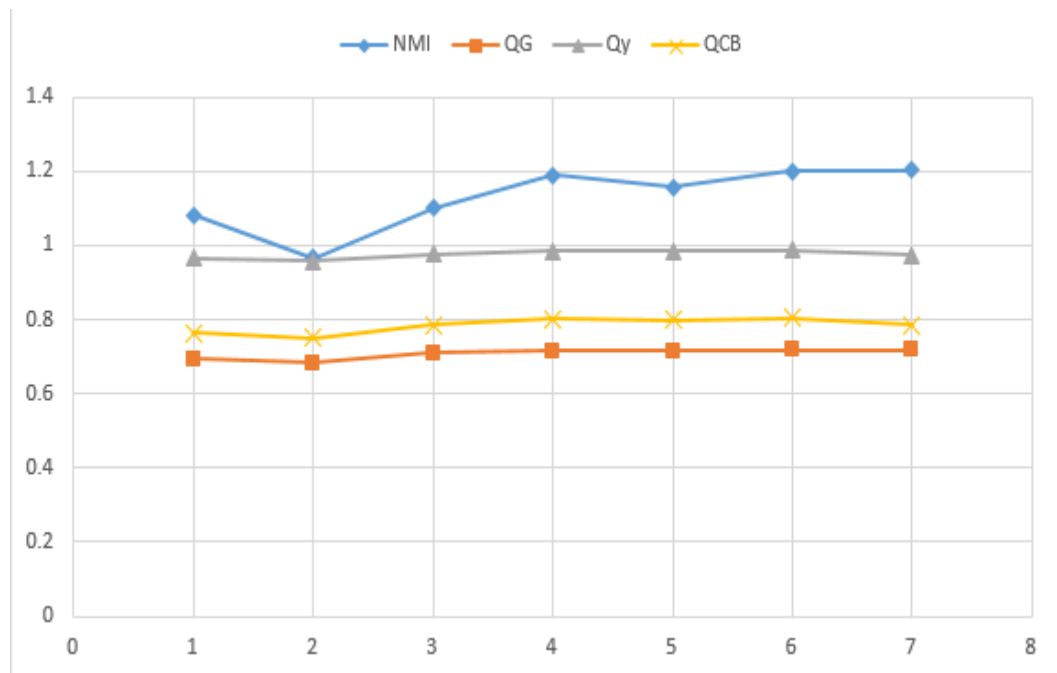FIGURE 4.4: Graph of Previous Techniques and Proposed Technique where Threshold=0.0001.

In this experiment, The threshold against 0.00007 less significant results but better than the some of the previous techniques. The threshold 0.00007 obtained better results as compared with our previous thresholds. It contain minimum defocus region that is way it perform better than the previous thresholds.

TABLE 4.5: Results of Previous Techniques and Proposed Technique where Threshold=0.00007.

Metrics	SR[38]	NSCT-SR[21]	GF[26]	DSIFT[22]	CNN[20]	DNN[19]	Proposed
NMI	1.0807	0.9651	1.1001	1.1902	1.1561	1.2002	**1.2029**
QG	0.6944	0.6823	0.7104	0.7162	0.7155	0.7188	**0.7208**
Qy	0.9663	0.9578	0.9775	0.9841	0.9851	**0.9871**	0.9769
QCB	0.7641	0.7499	0.7848	0.8005	0.8000	**0.8042**	0.8012

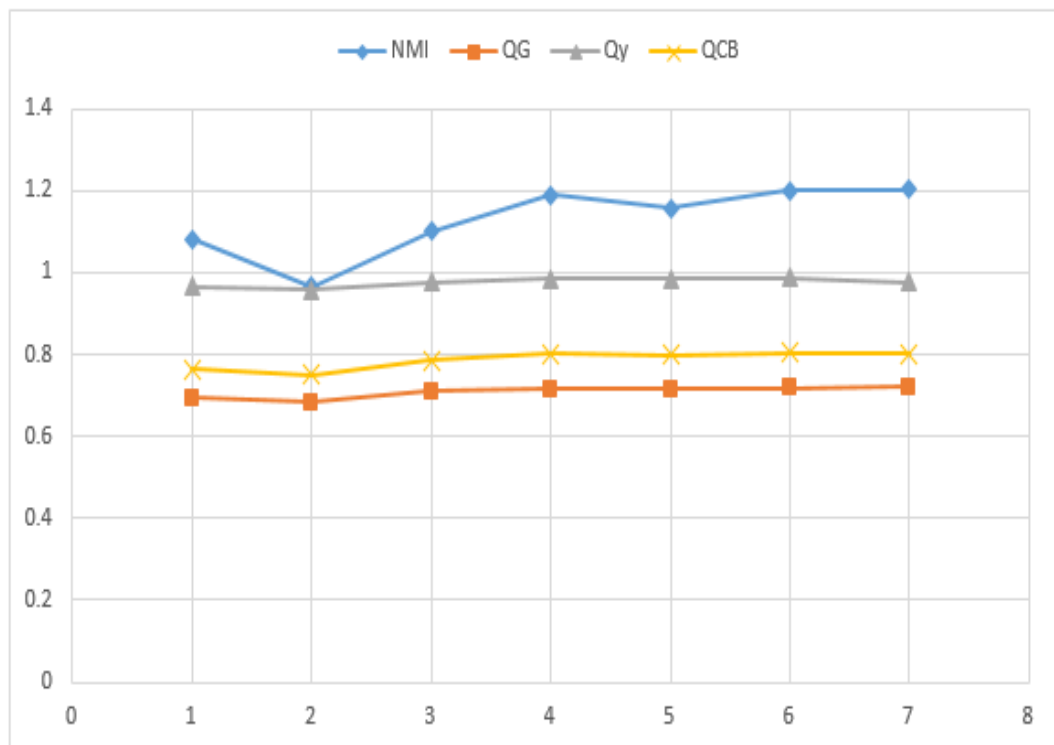FIGURE 4.5: Graph of Previous Techniques and Proposed Technique where Threshold=0.00007.

In this experiment, the threshold against 0.00005 provides significant results. All the results are not better than the previous techniques but maximum results are better than the previous techniques. The threshold 0.00005 obtained better results because its focus regions are more then the previous thresholds. According to the

results of 0.00005 thresholds some results are better and some are the similar to the previous techniques

TABLE 4.6: Results of Previous Techniques and Proposed Technique where Threshold=0.00005.

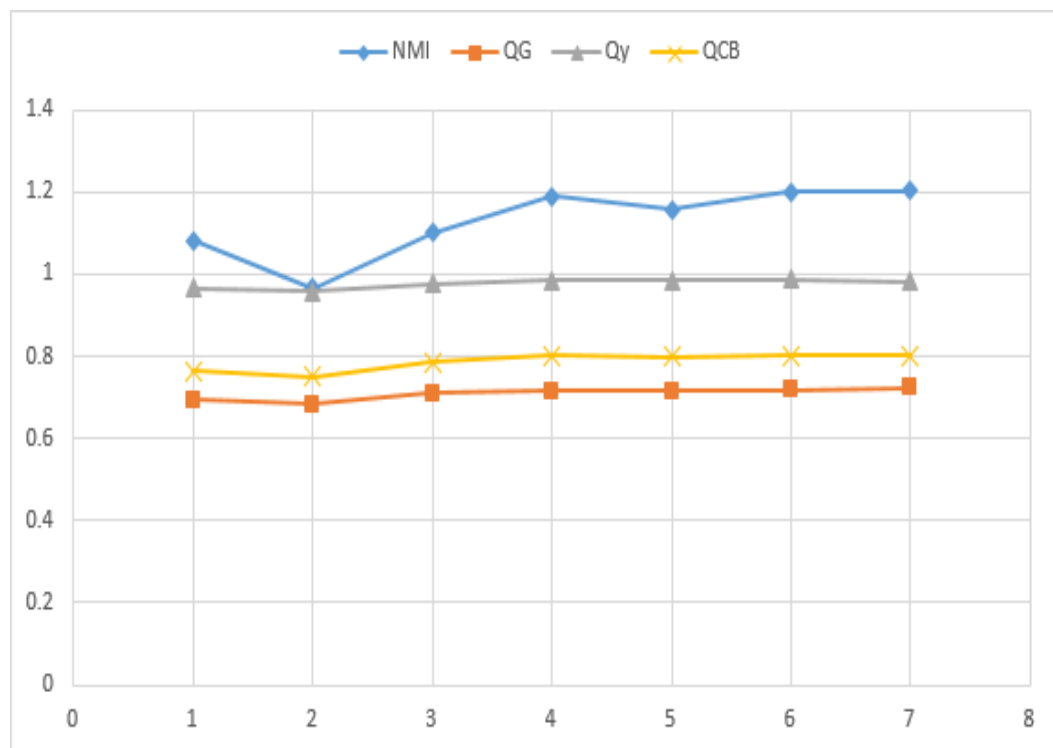| Metrics	SR[38]	NSCT-SR[21]	GF[26]	DSIFT[22]	CNN[20]	DNN[19]	Proposed
NMI	1.0807	0.9651	1.1001	1.1902	1.1561	1.2002	**1.2029**
QG	0.6944	0.6823	0.7104	0.7162	0.7155	0.7188	**0.7227**
Qy	0.9663	0.9578	0.9775	0.9841	0.9851	**0.9871**	0.9821
QCB	0.7641	0.7499	0.7848	0.8005	0.8000	**0.8042**	0.8024

FIGURE 4.6: Graph of Previous Techniques and Proposed Technique where Threshold=0.00005.

In this experiment, the results against threshold 0.00002 provides more significant and accurate. All the results are perform better than the previous techniques.

The threshold 0.00002 obtained better results because its focus regions are more than the previous thresholds. According to the results of threshold 0.00002 all the results perform well as compared with the previous techniques.

TABLE 4.7: Results of Previous Techniques and Proposed Technique where Threshold=0.00002.

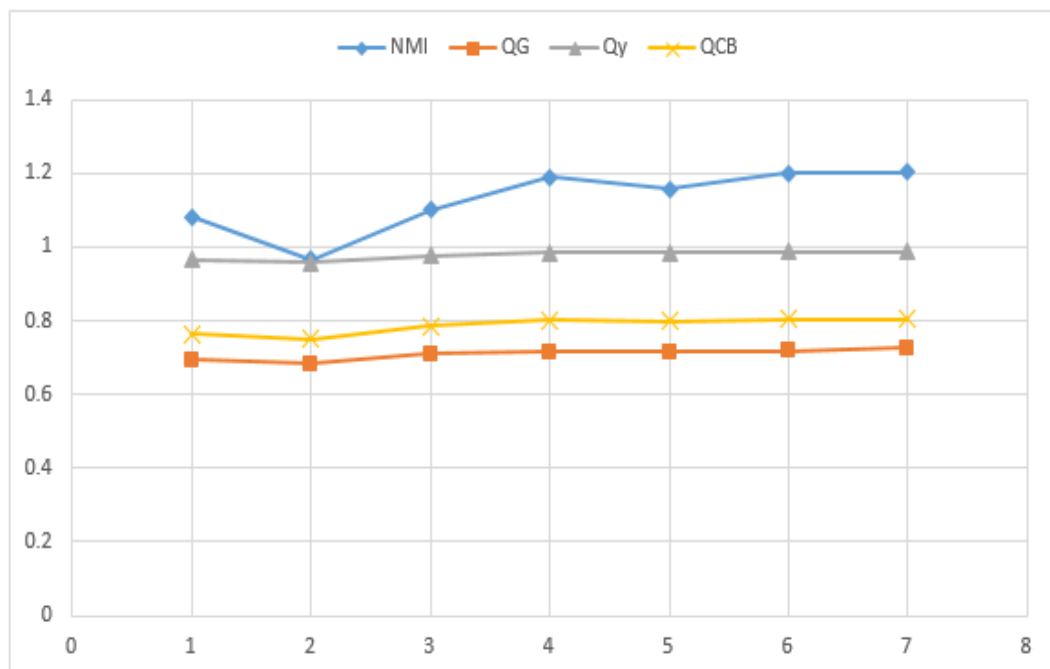| Metrics	SR[38]	NSCT-SR[21]	GF[26]	DSIFT[22]	CNN[20]	DNN[19]	Proposed
NMI	1.0807	0.9651	1.1001	1.1902	1.1561	1.2002	**1.2030**
QG	0.6944	0.6823	0.7104	0.7162	0.7155	0.7188	**0.7272**
Qy	0.9663	0.9578	0.9775	0.9841	0.9851	0.9871	**0.9873**
QCB	0.7641	0.7499	0.7848	0.8005	0.8000	0.8042	**0.8050**

FIGURE 4.7: Graph of Previous Techniques and Proposed Technique where Threshold=0.00002.

Chapter 5

Conclusion and Future Work

In this research, fused images are created using LBP based blur measure operator in multiple steps. In the first step, a blur measure operator is used to segment an input image. A segmented image contains a detail of blurred and non-blurred regions. In LBP, a grey value of a neighboring pixel corresponds to a grey level value of a central pixel. If the grey value of a neighboring pixel is not related to the central pixel then the pixel is estimated using interpolation. LBP is a texture-based operator that shows the occurrences of multiple binary patterns in neighborhoods of every pixel. In the last step, a fusion process is initiated where images are fused based on segmented maps.

In this experimentation, multiple varying thresholds are employed to segment an image. Fused images are evaluated using four qualitative measures such as NMI, Gradient, Yang, and Chen Blum. According to experimental results, a smaller threshold corresponds to better results as compared with higher thresholds. This technique is compared with 6 other techniques including sparse representation, a combination of non-subsampled contourlet transform and sparse representation, convolutional neural network, deep neural network, dense scale-invariant feature transform, and guided filer. Experimental results explain that the presented technique has outperformed previous state-of-the-art methods quantitatively.

Bibliography

[1] M. Sumathi and R. Barani, "Qualitative evaluation of pixel level image fusion algorithms," in *International Conference on Pattern Recognition, Informatics and Medical Engineering (PRIME-2012)*. IEEE, 2012, pp. 312–317.

[2] J. Dai, Y. Liu, J. He, X. Mao, G. Sheng, and X. Jiang, "Infrared and visible image fusion of electric equipment using fdst and dc-pcnn," in *2018 Condition Monitoring and Diagnosis (CMD)*. IEEE, 2018, pp. 1–6.

[3] V. Rubeena and K. Tiwari, "Multisensor multiresolution data fusion for improvement in classification," in *Multispectral, Hyperspectral, and Ultraspectral Remote Sensing Technology, Techniques and Applications VI*, vol. 9880. International Society for Optics and Photonics, 2016, p. 98800X.

[4] C. Morris and R. Rajesh, "A novel and improved spatial domain fusion method using simplepca techniques," in *2014 International Conference on Communication and Network Technologies*. IEEE, 2014, pp. 90–94.

[5] A. Patel and J. Chaudhary, "A review on infrared and visible image fusion techniques," in *Intelligent Communication Technologies and Virtual Mobile Networks*. Springer, 2019, pp. 127–144.

[6] J. Kaur, S. Sharma, and S. Gupta, "A novel technique for medical image fusion using improved contourlet transformation with modified dfbs," in *2013 Fourth International Conference on Computing, Communications and Networking Technologies (ICCCNT)*. IEEE, 2013, pp. 1–5.

[7] S. Li, Z. Li, and J. Gong, "Multivariate statistical analysis of measures for assessing the quality of image fusion," *International Journal of Image and Data Fusion*, vol. 1, no. 1, pp. 47–66, 2010.

[8] Z. Wang, L. Chen, J. Li, and Y. Zhu, "Multi-focus image fusion with random walks and guided filters," *Multimedia Systems*, vol. 25, no. 4, pp. 323–335, 2019.

[9] A. E. Hassanien, M. Elhoseny, S. H. Ahmed, and A. K. Singh, *Security in smart cities: models, applications, and challenges.* Springer, 2019.

[10] M. S. Holia and V. Thakar, "Mutual information based image registration for mri and ct scan brain images," in *2012 International Conference on Audio, Language and Image Processing.* IEEE, 2012, pp. 78–83.

[11] M. Abhyankar, A. Khaparde, and V. Deshmukh, "Spatial domain decision based image fusion using superimposition," in *2016 IEEE/ACIS 15th International Conference on Computer and Information Science (ICIS).* IEEE, 2016, pp. 1–6.

[12] G. Anbarjafari and H. Demirel, "Image super resolution based on interpolation of wavelet domain high frequency subbands and the spatial domain input image," *ETRI journal*, vol. 32, no. 3, pp. 390–394, 2010.

[13] V. Aslantas and R. Kurban, "Fusion of multi-focus images using differential evolution algorithm," *Expert Systems with Applications*, vol. 37, no. 12, pp. 8861–8870, 2010.

[14] W. Zhao, D. Wang, and H. Lu, "Multi-focus image fusion with a natural enhancement via a joint multi-level deeply supervised convolutional neural network," *IEEE Transactions on Circuits and Systems for Video Technology*, vol. 29, no. 4, pp. 1102–1115, 2018.

[15] W. Wang and F. Chang, "A multi-focus image fusion method based on laplacian pyramid." *JCP*, vol. 6, no. 12, pp. 2559–2566, 2011.

[16] J. Zhang, X. Feng, B. Song, M. Li, and Y. Lu, "Multi-focus image fusion using quality assessment of spatial domain and genetic algorithm," in *2008 conference on Human System interactions*. IEEE, 2008, pp. 71–75.

[17] R. Garg, P. Gupta, and H. Kaur, "Survey on multi-focus image fusion algorithms," in *2014 Recent Advances in Engineering and Computational Sciences (RAECS)*. IEEE, 2014, pp. 1–5.

[18] L. Cao, L. Jin, H. Tao, G. Li, Z. Zhuang, and Y. Zhang, "Multi-focus image fusion based on spatial frequency in discrete cosine transform domain," *IEEE signal processing letters*, vol. 22, no. 2, pp. 220–224, 2014.

[19] H. Ma, J. Zhang, S. Liu, and Q. Liao, "Boundary aware multi-focus image fusion using deep neural network," in *2019 IEEE International Conference on Multimedia and Expo (ICME)*. IEEE, 2019, pp. 1150–1155.

[20] Y. Liu, X. Chen, H. Peng, and Z. Wang, "Multi-focus image fusion with a deep convolutional neural network," *Information Fusion*, vol. 36, pp. 191–207, 2017.

[21] Y. Liu, S. Liu, and Z. Wang, "A general framework for image fusion based on multi-scale transform and sparse representation," *Information fusion*, vol. 24, pp. 147–164, 2015.

[22] ——, "Multi-focus image fusion with dense sift," *Information Fusion*, vol. 23, pp. 139–155, 2015.

[23] W. Huang and Z. Jing, "Evaluation of focus measures in multi-focus image fusion," *Pattern recognition letters*, vol. 28, no. 4, pp. 493–500, 2007.

[24] X. Zhang, X. Li, Z. Liu, and Y. Feng, "Multi-focus image fusion using image-partition-based focus detection," *Signal processing*, vol. 102, pp. 64–76, 2014.

[25] P. Jagalingam and A. V. Hegde, "A review of quality metrics for fused image," *Aquatic Procedia*, vol. 4, no. Icwrcoe, pp. 133–142, 2015.

[26] S. Li, X. Kang, and J. Hu, "Image fusion with guided filtering," *IEEE Transactions on Image processing*, vol. 22, no. 7, pp. 2864–2875, 2013.

[27] U. Ali and M. T. Mahmood, "Analysis of blur measure operators for single image blur segmentation," *Applied Sciences*, vol. 8, no. 5, p. 807, 2018.

[28] V. T. Hoang, A. Porebski, N. Vandenbroucke, and D. Hamad, "Lbp histogram selection based on sparse representation for color texture classification." in *VISIGRAPP (4: VISAPP)*, 2017, pp. 476–483.

[29] X. Yi and M. Eramian, "Lbp-based segmentation of defocus blur," *IEEE transactions on image processing*, vol. 25, no. 4, pp. 1626–1638, 2016.

[30] "http://mansournejati.ece.iut.ac.ir/content/lytro-multi-focus-dataset."

[31] C. Xydeas, , and V. Petrovic, "Objective image fusion performance measure," *Electronics letters*, vol. 36, no. 4, pp. 308–309, 2000.

[32] B. Bondžulić and V. Petrović, "Objective image fusion performance measures," *Vojnotehnički glasnik*, vol. 56, no. 2, pp. 181–193, 2008.

[33] M. B. A. Haghighat, A. Aghagolzadeh, and H. Seyedarabi, "A non-reference image fusion metric based on mutual information of image features," *Computers & Electrical Engineering*, vol. 37, no. 5, pp. 744–756, 2011.

[34] A. A. Kiaei, H. Khotanlou, M. Abbasi, P. Kiaei, and Y. Bhrouzi, "An objective evaluation metric for image fusion based on del operator," *arXiv preprint arXiv:1905.07709*, 2019.

[35] Z. Zhou, S. Li, and B. Wang, "Multi-scale weighted gradient-based fusion for multi-focus images," *Information Fusion*, vol. 20, pp. 60–72, 2014.

[36] Y. Chen and R. S. Blum, "A new automated quality assessment algorithm for image fusion," *Image and vision computing*, vol. 27, no. 10, pp. 1421–1432, 2009.

[37] C. Yang, J.-Q. Zhang, X.-R. Wang, and X. Liu, "A novel similarity based quality metric for image fusion," *Information Fusion*, vol. 9, no. 2, pp. 156–160, 2008.

[38] B. Yang and S. Li, "Multifocus image fusion and restoration with sparse representation," *IEEE Transactions on Instrumentation and Measurement*, vol. 59, no. 4, pp. 884–892, 2009.